


# Feasibility of Enhancing Skin Permeability of Acyclovir through Sterile Topical Lyophilized Wafer on Self-Dissolving Microneedle-Treated Skin

Dose-Response:  
An International Journal  
April-June 2022:1–21  
© The Author(s) 2022  
Article reuse guidelines:  
[sagepub.com/journals-permissions](https://sagepub.com/journals-permissions)  
DOI: 10.1177/15593258221097594  
[journals.sagepub.com/home/dos](https://journals.sagepub.com/home/dos)  


Uzair Nagra<sup>1,2</sup>, Kashif Barkat , Muhammad U Ashraf<sup>2</sup>, and Maryam Shabbir<sup>2</sup>

## Abstract

Acyclovir is an antiviral drug that is frequently prescribed for the herpes virus. However, the drug requires frequent dosing due to limited bioavailability (10–26.7%). The rationale of the present study was to develop a self-dissolving microneedle system for local and systemic delivery of acyclovir using a topical lyophilized wafer on microneedle-treated skin to provide the drug at the site of infection. The microneedles prepared with hydroxypropyl methylcellulose (HPMC) (8% w/w) or HPMC (8% w/w)-polyvinyl pyrrolidone (PVP) (30% w/w) penetrated excised rat skin, showing sufficient mechanical strength and rapid polymer dissolution. The topical wafer was prepared with acyclovir (40% w/w; equivalent to 200 mg of drug), gelatin (10% w/w), mannitol (5% w/w), and sodium chloride (5% w/w). The uniform distribution of acyclovir within the wafer in an amorphous form was confirmed by differential scanning calorimetry (DSC) and thermogravimetric analysis (TGA). No polymer–drug interaction was evident in the lyophilized wafer as per Fourier transform infrared spectroscopy (FTIR) analysis. The wafer showed a sufficiently porous structure for rapid hydration as per scanning electron microscopy (SEM) analysis. During *ex-vivo* analysis, the skin was pre-treated with a self-dissolving microneedle array for 5 minutes, and the wafer was placed on this microporated-skin. Topical wafer provided ~7–11 times higher skin concentration than the ID<sub>99</sub> reported with a lower lag-time. Based on *in-vivo* testing, ~2.58 µg/ml of C<sub>max</sub> was achieved in rabbit plasma during 24 hours' study. Our findings suggest that the self-dissolving microneedle-assisted topical wafer, proposed for the first time, would be efficacious against the infection residing in the skin layer and for systemic therapy.

## Keywords

Acyclovir, microneedle, polymer dissolution, skin permeation, topical lyophilized wafer

## Introduction

The *Herpesviridae* is a large family of viral-DNA that causes disease in both humans and animals. The hallmark of the human herpesvirus (HHV) is its ability to maintain a lifelong latent infection phase in the host. Therefore, the herpes virus can be easily called an opportunistic pathogen that tends to reactivate in immunocompromised patients.<sup>1</sup> Of all the herpes viruses, herpes simplex virus-1 (HSV-1) and HSV-2 are most closely related. Herpes simplex virus-1 is primarily associated with cold sores, or herpes labialis, on the lips. The HSV-2 is commonly associated with genital sores or genital herpes. However, both viruses can cause lesions at either site. The lesions subside after the

primary infection with proper treatment but might reappear later in life due to the latency of the virus within the body. Currently,

<sup>1</sup>Department of Pharmacy, The University of Lahore - New Campus, Lahore, Pakistan

<sup>2</sup>Department of Pharmacy, The University of Lahore, Lahore, Pakistan

Received 20 February 2022; received revised 13 March 2022; accepted 23 March 2022

### Corresponding Author:

Kashif Barkat, Faculty of Pharmacy, The University of Lahore, Lahore, Pakistan.

Email: [dr.kashif2009@gmail.com](mailto:dr.kashif2009@gmail.com)



Creative Commons Non Commercial CC BY-NC: This article is distributed under the terms of the Creative Commons Attribution-NonCommercial 4.0 License (<https://creativecommons.org/licenses/by-nc/4.0/>) which permits non-commercial use, reproduction and distribution of the work without further permission provided the original work is attributed as specified on the SAGE

and Open Access pages (<https://us.sagepub.com/en-us/nam/open-access-at-sage>).

the only definitive treatment of HSV is acyclovir. Acyclovir falls in BCS Class III with poor permeability characteristics. The oral bioavailability of acyclovir varies considerably in humans (10–26.7%).<sup>2</sup> Different routes of administrations have been exploited for the delivery of acyclovir in herpes virus infection (HVI). For instance, the oral route and parenteral route have been extensively studied for immunocompetent and immunocompromised hosts for both treatment and prophylaxis of HVI. However, due to a shorter half-life, it requires repeated administration at a high dose for effective management.<sup>3</sup> For example, for the treatment of acute herpes zoster infection, 800 mg of oral acyclovir is recommended every 4 hours, 5 times a day for a total of 7–10 days. For the intermittent therapy of genital herpes, 200 mg of oral acyclovir is recommended every 4 hours, 5 times daily for 5 days.<sup>4</sup> Topical application is widely used for the treatment of various HVIs including herpes simplex keratitis on the cornea, lip, and vaginal pathologies. Still, the topical acyclovir formulation has not shown promising clinical benefits in recurrent herpes labialis.<sup>5</sup> This limitation of topical application is attributed to the polarity of the drug ( $-1.76$  at pH 7) which hinders the partitioning of acyclovir in aqueous and lipid media of the stratum corneum. Thus, passive delivery of acyclovir across the skin requires a frequent and long-term application for the treatment of cold sores.<sup>6</sup> The frequency of administration is undoubtedly an inconvenience in the acyclovir treatment strategy. Therefore, it is suggested to change the drug delivery system to achieve targeting of a drug in the skin and systematically.

Lyophilized wafers are a highly porous solid matrix system obtained after freeze-drying of drug–polymer suspensions to form small disks or thin films. There are many oral lyophilizates commercially available in the market such as Zydis<sup>®</sup> and Quicksolv<sup>®</sup> technology.<sup>7</sup> However, such a concept has not gained much recognition in the transdermal drug delivery system. Therefore, the present study explores the possibility of using lyophilized wafers on microneedle-treated skin to enhance the permeation of the antiviral drug acyclovir across the stratum corneum. The terms like a lyophilized wafer, topical lyophilizate, and drug-reservoir are used interchangeably.

We describe, for the first time, the use of topical lyophilized wafer for the delivery of high-dose acyclovir through micropores generated in self-dissolving polymeric microneedle-treated skin. Usually, the microneedle treatment is done with silicon or metal microneedles (poke and patch approach) to enhance the delivery of drugs across the skin. However, we report the use of hydrophilic, biocompatible, and biodegradable polymers to serve the same purpose to overcome the limitations posed by solid-metal microneedles. The general approach follows that presented by Nguyen et al (2018)<sup>8</sup> and Qian et al (2014)<sup>9</sup> who pre-treated the skin with polyvinyl alcohol (PVA)-based polymeric microneedle for the delivery of doxorubicin (poke and solution) and sinomenine (microemulsion-based gel), respectively. Recently, acyclovir-loaded dissolving microneedles have been reported by Pamornpahomkul et al, (2018) using Gantrez S-97 as a polymeric base material.<sup>10</sup> The lyophilized wafers are routinely reported

with the use of hydrogel/super-swelling microneedles where the swelling of the matrix aids in the passage of the drug through the micropores.<sup>11–13</sup> But it is usually accompanied by a longer lag time because of the time required for fluid uptake and the process of hydrogel swelling to allow the passage of drug from the wafer into the skin. Moreover, the drug permeation might also be affected by diffusion and partitioning of the drug in and out of the hydrogel.<sup>13</sup> Therefore, we propose the formation of micropores in the epidermis before the application of topical lyophilized wafers to possibly provide large-dose acyclovir for possible treatment of herpes infection with reduced lag time.

## Materials and Method

### Materials and Animal Husbandry

Acyclovir was a gift from Medisearch Pharmaceuticals Pvt. Ltd. (Lahore, Pakistan). Polyvinyl alcohol, polyvinyl pyrrolidone (PVP), hydroxypropyl methylcellulose (HPMC), and gelatin were purchased from Sigma-Aldrich. Disodium hydrogen phosphate, potassium dihydrogen phosphate, and sodium chloride were purchased from Merck, Germany. Acetonitrile was purchased from Merck, Germany, and distilled water was prepared in the Research Laboratory of Faculty of Pharmacy, The University of Lahore, Lahore, Pakistan. The microneedle template (Smicna Pte, Ltd., Singapore) comprised 225 (15 x 15) needle holes on a .64-cm<sup>2</sup> area, perpendicular to the base. The micro-holes had a height of 600  $\mu$ m, needle base of 200  $\mu$ m with interspacing of 500  $\mu$ m, and pyramidal shape.

The animal handling and procedures were taken and approved by the Institutional Research Ethical Committee (IREC), Faculty of Pharmacy, The University of Lahore, Lahore, under consent number IREC-2020-26. The animals were housed according to the standard protocol of 12:12 hour light–dark cycle in a temperature-controlled room of  $25 \pm 2^\circ\text{C}$ . They were provided with food and water *ad libitum*. Any animal with 20% weight loss during the study was to be removed for euthanizing, but this did not occur during the experimental protocol adapted.

### Preparation of Dissolving Polymeric Microneedle

Based on the preliminary analysis, HPMC and PVP were selected for the formation of dissolving microneedles through the solvent evaporation technique. For HPMC solution (8% w/w), a defined amount of polymer was placed in 10 mL of distilled water (preheated at  $40 \pm 2^\circ\text{C}$ ) and stirred to obtain a clear solution. The resulting solution was stored for 24 hours for complete hydration before microneedle processing. For the baseplate formation, a defined amount of PVA (15% w/v) was added in 10 mL of distilled water. The beaker was placed in a water bath (Jisico Co. Ltd., South Korea) preset at  $60 \pm 1^\circ\text{C}$  and allowed to disperse for 6 hours. For the co-mixture of HPMC and PVP, a defined amount of PVP (30% w/v) was

added in the previously prepared HPMC (8% w/v) solution and allowed to mix homogeneously on a magnetic stirrer (Jisico Co. Ltd., South Korea). Before the fabrication process, all polymer solutions were centrifuged at 3500 r/min for 5 minutes to remove the entrapped air bubbles.<sup>14</sup> The polymer blends were stored at room temperature in sealed containers and occasionally checked for stability.

For the formation of HPMC-based microneedles (formulation code: UN-1), a two-layer procedure was adopted. The micro-tips of UN-1 were prepared by dosing approximately .11–.15 g of HPMC (8% w/w) onto the microneedle template and centrifuged for 5 minutes at 3500 rpm. After centrifugation, the PVA (15% w/w) solution was poured on the template surface for the formation of the baseplate. The templates were placed in a closed container and allowed to dry for 24 hours at  $32 \pm 2^\circ\text{C}$  in a desiccator (Pol-Eko-Aparatura, Poland). Finally, the microneedles were removed from the template and stored till further analysis. For the formation of HPMC (8% w/w)-PVP (30% w/w)-based microneedles (formulation code: UN-2), a one-layer method was used, that is, the micro-tip and baseplate composed of the same polymer matrix. The microneedles were prepared with the same procedure as stated previously.

### *Physical and Morphological Characterization of Microneedles*

To ensure the uniformity, methylene blue (1% w/v) dye was added to the polymeric solution. Methylene blue containing UN-1 and UN-2 microneedles were fabricated as described before and visualized under the light microscope (XSZ-107BN, China). The dimensions of the microneedle array were assessed using the imaging software, Image J.<sup>15</sup>

### *Mechanical Strength Test of Dissolving Microneedle*

To estimate the static mechanical strength test, different weights were placed on the tips of the microneedle array to determine the degree of deformation. The microneedles were placed under the thin sheet of aluminum, and weights of 10, 20, 50, and 100 g were placed on top of the arrays and held for 5 minutes, respectively. After each weight, the microneedles were examined under the light microscope and photographed to analyze the bending of the microneedle tip.<sup>16,17</sup> Three distinct failure modes were observed to characterize the behavior of mechanical strength, including (a) failure in bending of the tip, (b) failure due to abrupt failure, and (c) failure due to bulking.<sup>18</sup>

### *Insertion Depth of Dissolving Microneedle in Parafilm® M*

The insertion depth of dissolving microneedles was assessed through artificially simulated skin Parafilm® M. The film was

folded 8 times, and a microneedle was placed above the first layer. The array was pierced into the layers with a thumb pressure to facilitate insertion into the film. Post-insertion, the microneedle was viewed under the digital microscope to observe the tip bending and associated morphological changes. Afterward, each layer of Parafilm® M was examined under the digital microscope to count the number of holes formed by the microneedle. Insertion in each layer was regarded as successful if the number of microholes was greater than 20%. The insertion depth was estimated with reference to the thickness of a single layer of film.<sup>19</sup>

### *Ex Vivo Polymer Dissolution Studies of Dissolving Microneedle*

To obtain the full-thickness skin, the hair on the rabbit was trimmed and shaved under anesthesia. The animals were later euthanized by cervical dislocation, and full-thickness skin was obtained. After removing the subcutaneous fats with alcohol swabs, the skin was washed, dipped in normal saline solution, and refrigerated till further testing.<sup>20</sup> The excised skin was wrapped in aluminum foil and kept at  $-20^\circ\text{C}$ , if required.<sup>20</sup> Initially, the microneedle was photographed under the light microscope at the time: 0 minutes. Later, the dissolving microneedle was applied to the shaved skin using firm finger pressure for 30 seconds. After a suitable time interval of 2, 5, and 10 minutes, the microneedle array was removed from the skin surface and analyzed under the light microscope for imaging the residual height of microneedle tips.<sup>16,20</sup>

### *Skin Insertion Studies on Rabbit Skin and Staining*

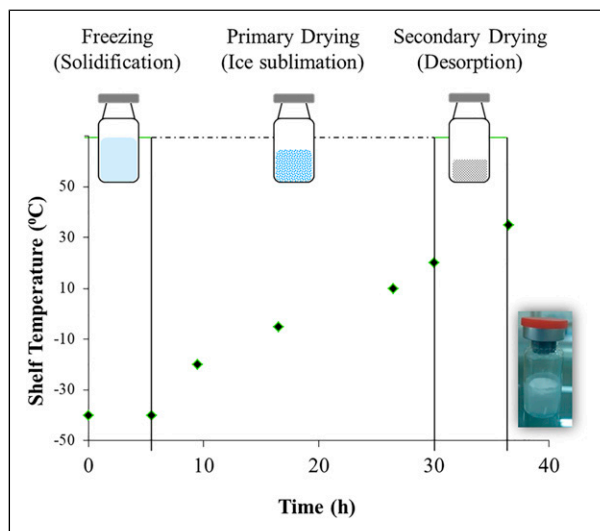
For histological sections, the microneedle-treated skin was fixed in 10% formalin solution for at least 24 hours before rinsing with phosphate buffer saline (PBS pH, 7.4) solution. The skin was later sliced into thick sections, and was surface stained with eosin and hematoxylin. The prepared histological slides were viewed under a light microscope and photographed.<sup>21</sup> Alternatively, the skin was stained with methyl blue solution (.1% w/v) for 10 minutes to estimate the sustenance of pore over a 12-hour period. The excess dye was wiped with isopropyl alcohol (IPA) and gently washed out using PBS (pH, 7.4) for a photograph.<sup>14,22</sup>

### *Preparation of Acyclovir-Loaded Topical Lyophilized Wafer*

The topical lyophilized wafer of acyclovir was prepared and packaged under sterilized conditions. Briefly, acyclovir, gelatin, mannitol, and sodium chloride were blended in distilled water as given in Table 1.<sup>11,12</sup> The formulation was then mixed by a homogenizer (DLAB: D-160 Homogenizer, Dr Lab Technology, Hong Kong) at 2000 rpm for 60 seconds and sonicated (Labtech Scientific, Italy) for 60 minutes at room

**Table I.** Formulation of Topical Lyophilized Wafer of Acyclovir.

Formulation code	Drug (% w/w)	Gelatin (% w/w)	Mannitol (% w/w)	Sodium chloride (% w/w)
F1	40	10	5	–
F2	40	10	5	5
F3	40	15	5	5
F4	35	15	5	5

**Figure 1.** Schematic illustration of sterile preparation of topical lyophilized wafer of acyclovir in freeze-dryer with an embedded image of the final formulations (LVV-2).

temperature. The resulting acyclovir formulation (equivalent to 200 mg of drug) was cast in a glass vial loaded in the bottom-shelf of the freeze-drier (LYO-10.0-CIP-SIP, Tofflon, China) as shown in Figure 1. The initial freezing was carried out at  $-40^{\circ}\text{C}$  for at least 5.5 hours without generating any vacuum pressure. After the stated time, the lyophilization cycle entered into the following regimen: primary drying at  $-20^{\circ}\text{C}$  for 4 hours (1 Torr pressure),  $-5^{\circ}\text{C}$  for 7 hours (.75 Torr pressure), and  $10^{\circ}\text{C}$  for 8 hours (.75 Torr pressure) and secondary drying at  $20^{\circ}\text{C}$  for 3.5 hours (.3 Torr pressure) and  $35^{\circ}\text{C}$  for 6.5 hours (.1 Torr pressure). After the freeze-drying process, the auto-cycle stopped and ejected the sealed glass vials containing topical lyophilized wafers.

#### Physical Characteristics and Content Uniformity in Acyclovir-Loaded Topical Lyophilized Wafer

Lyophilized drug reservoirs of lead formulation were characterized for standard pharmacopeia tests including weight variation, thickness, and diameter. For weight uniformity, twenty wafers were randomly selected from a batch and weighed individually on a digital weighing balance (Ohaus, China). The percentage deviation of each wafer was estimated from the average weight as per following equation

$$\text{Weight variation (\%)} = \left( \frac{\text{Average weight} - \text{Individual weight}}{\text{Average weight}} \right) \times 100$$

The thickness and diameter of a lyophilized wafer ( $n = 10$ ) were taken with a digital Vernier caliper (Dasqua, Italy) to estimate the average and standard deviation.<sup>23</sup>

The drug content in the topical lyophilized wafer was determined by dissolving the dosage form in 500 mL of phosphate buffer saline (PBS pH 7.4). The formulation was stirred on a magnetic stirrer at 600 rpm to ensure complete mixing. Afterward, samples withdrawn were diluted appropriately and analyzed using UV/vis-spectroscopic detection (Shimadzu, Germany) at 254 nm.<sup>24</sup>

#### Scanning Electron Microscopy Analysis of Acyclovir Containing Lyophilized Wafer

Scanning electron microscopy (SEM) (Exo LS 10, Zeiss, Germany) was used to analyze the surface morphology of the wafer at low accelerating voltage. The wafer was cut into smaller pieces and attached to the aluminum stubs with the aid of double-sided adhesive tape. Afterward, the wafer was visualized in the microscope, and images were captured at different magnifications. Similarly, the microneedle was viewed under SEM to capture the needle structure.<sup>25</sup>

#### Analysis of Chemical Composition by Fourier Transform Infrared Spectroscopy

Fourier transform infrared spectroscopy (FTIR) analysis was carried out to confirm the purity and presence of functional groups of polymers, drug, and lyophilized wafer. The infrared spectra of the samples were analyzed within the wavenumber range of  $4000\text{--}600\text{ cm}^{-1}$  using a PerkinElmer Frontier FTIR.<sup>26</sup>

#### Differential Scanning Calorimetry Analysis of Acyclovir Containing Lyophilized Wafer

The differential scanning calorimetry (DSC) apparatus was calibrated with the melting temperature of Indium at  $156.5^{\circ}\text{C}$ . The DSC studies of acyclovir, polymers, and physical mixture of polymers were carried with a TA Instruments Q2000 series Thermal Analysis System. The sample was weighed between 4–5 mg and sealed in non-hermetic-type aluminum pans. The

temperature was ramped up at a heating rate of 10°C/minute in presence of nitrogen purge in the temperature range of 25–500°C.<sup>27</sup>

### Thermogravimetric Analysis of Acyclovir Containing Lyophilized Wafer

The thermogravimetric (TGA) studies of acyclovir, polymers, and physical mixture of polymers were carried with TA instruments Q5000 series Thermal Analysis System (TA instruments, UK). The samples were analyzed under nitrogen purge whilst regulating the heating rate at 10°C/minute in the temperature range of 25–500°C.<sup>26</sup>

### Determination of Saturation Solubility of Acyclovir Using Flask-Shake Method

To estimate the saturation solubility of acyclovir, the drug was added in excess to 8 mL of solvents including (a) distilled water, (b) PBS (pH 7.4), (c) PBS and Tween 80 (.5% v/v), (d) PBS and Tween 80 (1.0% v/v), and (e) PBS and methanol (80:20). The separate glass vials containing the aforementioned solvents and drug were agitated on a thermostatically controlled orbital shaker at 200 r/min for 24 hours at 37 ± 2°C. After 24 hours, the sample was allowed to settle down. The supernatant solution was filtered through a .2-µm filter and analyzed on a UV-spectrophotometer at 254 nm.<sup>24</sup>

### Ex-Vivo Permeation Studies of Acyclovir Across Excised Rabbit Skin

The *ex-vivo* permeation studies of the topical lyophilized wafer across self-dissolving microneedle-treated skin were investigated on excised rabbit skin using the Franz diffusion cell (capacity: 12 mL, diffusion area: 1.76 sq. cm). To obtain the full-thickness skin, the skin was treated as described previously. Before the experiment, the receiver compartment was filled with PBS (pH, 7.4) containing 1.0% v/v Tween 80 to retain the drug solubility in the buffer and ensure sink conditions. The excised skin was first treated with dissolving microneedle for 5 minutes to generate the micropores and then mounted on the Franz diffusion cell. The topical lyophilized wafer (equivalent to 50 mg) was placed on top of the skin as shown in [Figure 2A](#). A similar experimental protocol was followed for commercially available cream in which the donor compartment was loaded with acyclovir topical cream (equivalent to 50 mg). In all cases, the donor compartment was clamped onto the receiver compartment and sealed with Parafilm® M. Sample was withdrawn after a suitable time interval, and fresh-prewarmed buffer was added into the receiver compartment.

On completion of the permeation studies, the skin was removed from the Franz diffusion cell, and the drug present on the skin surface was washed twice with 10 mL of fresh PBS (pH 7.4) and acetonitrile (1:1). The two pieces of washing were combined, and the drug retained on the skin surface was

quantified by the UV-spectrophotometric method at 254 nm. The tape stripping method (Scotch® Magic™ Tape, 3M) was used to detect the drug deposited in the stratum corneum layer. The skin was tape stripped 15 times and added to 20 mL of fresh PBS (pH 7.4) and acetonitrile (1:1) mixture and agitated for 24 hours for complete extraction. The sample was filtered, centrifuged and quantified spectrophotometrically. After surface drug washing and removal of the stratum corneum, the skin was minced in a chopper and collected in 8 mL of PBS (pH, 7.4) and acetonitrile (1:1). The material was homogenized for 5 minutes under cold conditions and subsequently vortexed for 10 minutes. The supernatant was collected after centrifugation of the material (5000 rpm for 10 minutes), and settled tissue debris was discarded. The percentage of drug deposited in the skin was quantified after the UV-spectrophotometric method.<sup>28</sup>

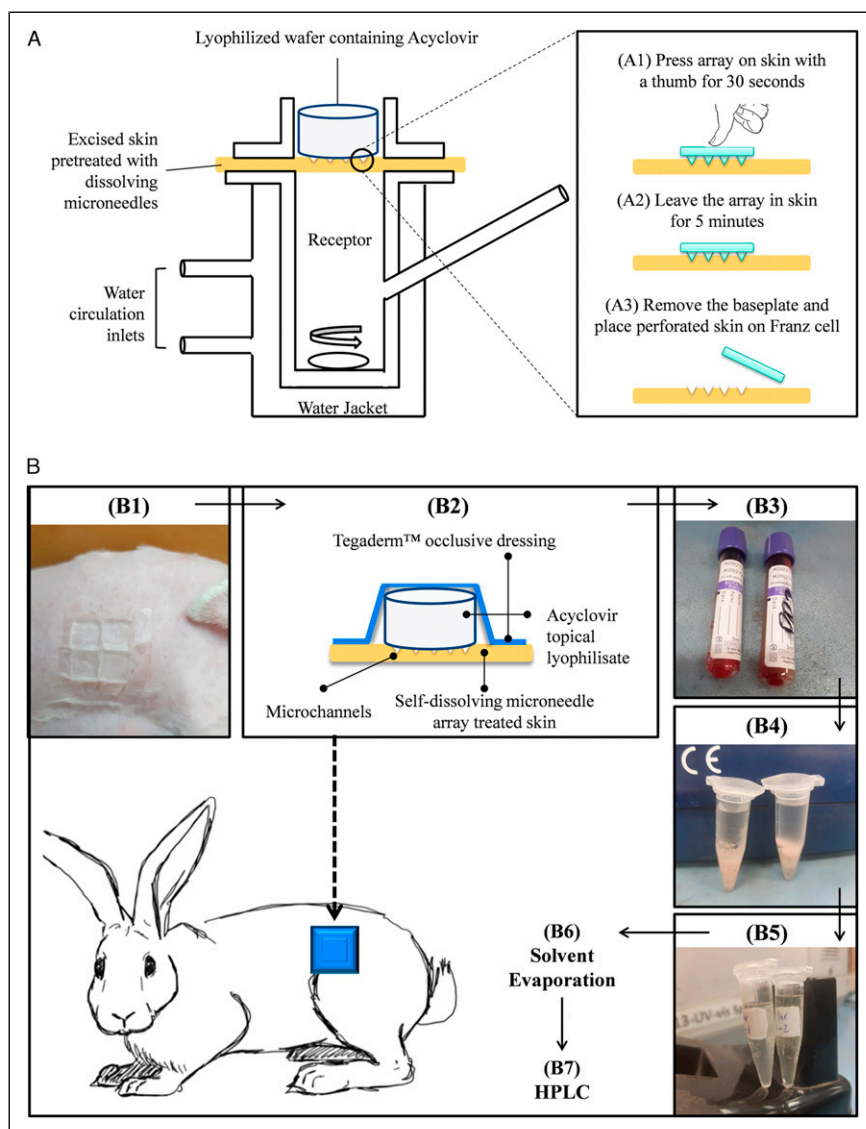
Data including cumulative amount (Q: µg and µg/sq.cm); percentage permeated at 24<sup>th</sup> hour, acyclovir steady-state flux ( $J_{ss}$ : µg/sq.cm.h); acyclovir retained in skin and stratum corneum (µg/sq.cm); acyclovir retained on the surface (µg/sq.cm); and permeation enhancement ratio (PER) were calculated.  $J_{ss}$  was estimated by taking the slope of the steady-state portion of the cumulative release (µg/sq.cm) profile. Permeation enhancement ratio of the self-dissolving microneedle-assisted topical lyophilized wafer as compared to marketed cream (control) was calculated from  $J_{ss}$ . The lag time (*x*-intercept) was calculated from the linear portion of the cumulative amount (µg/sq.cm) vs time (h) plot ( $y = 0$ ).<sup>29</sup>

### In Vivo Pharmacokinetic Analysis

The rabbits (weight: 1.5 kg) were housed according to the standard protocol of 12:12 hour light–dark cycle in a temperature-controlled room of 25 ± 2°C. For this, male rabbits were acclimatized with the laboratory conditions for 1 week before the experiment.<sup>30</sup> They were kept on a regular diet with close monitoring of their weight and behavior. Animals were anesthetized by gas anesthesia, and the abdominal area of rabbits was trimmed using an animal hair clipper (Bran Series Electric shaver). Afterward, the skin was treated with hair removal cream (Veet® for sensitive skin, Reckitt Benckiser, Pakistan) and kept for 5 minutes. The hairs were removed with a plastic spatula, and the skin was immediately washed with lukewarm water. The animals were left for one day before the experiment to ensure the complete removal of cream from the site of application.<sup>31</sup>

### Extraction of Rabbit Plasma and Acyclovir Quantification by HPLC

Before the application of a topical lyophilized wafer, the abdominal area of the rabbit was treated with an array (composed of 4 dissolving microneedles) for 5 minutes. The array was affixed on adhesive foam which was then secured on the pinched section of the skin with an aid of firm pressure. After 5 minutes, the array was removed from the skin, and a



**Figure 2.** (A) Setup of Franz diffusion cell for ex vivo permeation studies of the acyclovir lyophilized wafer across pre-treated excised rabbit skin. Step A1–A3 represent stratum corneum puncturing with self-dissolving microneedle array (UN-1; HPMC 8% w/w) before mounting the skin on Franz diffusion cell. (B) Schematic representation of acyclovir detection in blood after administration of topical lyophilized wafer on self-dissolving microneedle-treated skin: (B1) Pre-treatment of shaved skin of rabbit with a self-dissolving array consisting of 4 microneedles, (B2) application of topical acyclovir lyophilizate on microneedle-treated skin, (B3), blood sampling from marginal ear vein of rabbit after a suitable time interval, (B4) precipitation of protein by acetonitrile during vortexing and sedimentation through centrifugation, (B5) collection of drug-containing supernatant, (B6) evaporation of the solvent in a desiccator, and (B7) acyclovir quantification by HPLC.

topical lyophilized wafer was placed on the microneedle-treated area. To secure the wafer in place (acyclovir equivalent to 40 mg/kg), an occlusive dressing Tegaderm™ (3M, imported from the USA) was placed on top of the skin section as summarized in Figure 2B.<sup>32</sup>

The samples were immediately collected in EDTA tubes to prevent blood clots. Afterward, the blood samples were centrifuged at 5000 rpm in a refrigerated centrifugation machine (K3 Series, Centurion Scientific Ltd, UK) for 10 minutes. The plasma of 200 µl (2 samples from each blood extraction) was collected in 3-mL microtubes and treated with

1000 µl of acetonitrile. The microtubes were then vortexed for 10 minutes followed by centrifugation at 10 000 rpm for 60 seconds in a centrifugation machine at 25°C. The supernatant of the 2 microtubes of each time point was combined to make a 1000-µl drug-extracted sample. Subsequently, the solvent was evaporated in a desiccator preset at 40°C. A similar protocol was adopted for two more rabbits, and the drug was extracted from plasma as previously stated before reconstitution with the mobile phase for HPLC analysis.<sup>10,33</sup>

Acyclovir was quantified using HPLC (Shimadzu, Germany) with a UV-visible detector. The separation was performed in

isocratic mode using the Thermo Scientific Hypersil C-18 column. The avoid interference of plasma with acyclovir, the mobile phase was a gradient of acetonitrile and 5mM ammonium acetate buffer pH 4.0 at 60:40 v/v ratios with a flow rate of 1mL/minute. The detector wavelength was set at 250 nm, and the volume injected was 10  $\mu$ l using an autoinjector. The run time of samples was set at 10 minutes whilst the retention time of acyclovir was obtained at approximately 3.45 minutes.<sup>10</sup>

### Pharmacokinetic Parameters

The plasma data were modeled using pharmacokinetic software PKSolver.<sup>34</sup> Pharmacokinetic parameters were calculated from the plasma concentration-time curves for acyclovir including peak height (Cmax), peak time (Tmax), partial area under curve (AUC<sub>0-t</sub>), total area under curve (AUC<sub>0-∞</sub>), area under the moment curve (AUMC), mean absorption half-life (t<sub>1/2k<sub>a</sub></sub>), terminal half-life (t<sub>1/2k<sub>10</sub></sub>), volume of distribution (V/F), oral clearance (CL/F), and mean residence time (MRT).<sup>34</sup>

### Accelerated Stability Test

Accelerated stability tests for the topical lyophilized wafer and self-dissolving microneedle were conducted according to ICH and WHO guidelines. The stated formulations were stored at 40 ± 2°C, 75 ± 5% RH for 168 days in a constant climate chamber (Memmert GmbH+Co., Germany). To establish the stability profile of microneedles, the arrays were placed in a stability chamber with needle size facing downwards. The samples were taken out at pre-defined time intervals of 7, 28, 84, and 168 days and were not returned to the storage chamber. Any changes evident in the polymer distribution, contraction or bending of the baseplate, needle deformation or breakage, and color change were documented.<sup>35,36</sup> A similar method was adapted for topical lyophilized wafers, where the sterile product was checked for endotoxins, particulate matter, or signs of discoloration. The drug content in wafer was quantified at pre-defined intervals.<sup>36</sup>

**Statistical analysis.** Statistical analysis was performed using commercially available software MS Excel for the determination of mean and standard deviation. Where applicable, analyses of the result were undertaken using one-way analyses of variance (ANOVA). In each case,  $P < .05$  represented a statistically significant difference.


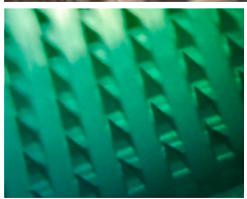
## Results and Discussion

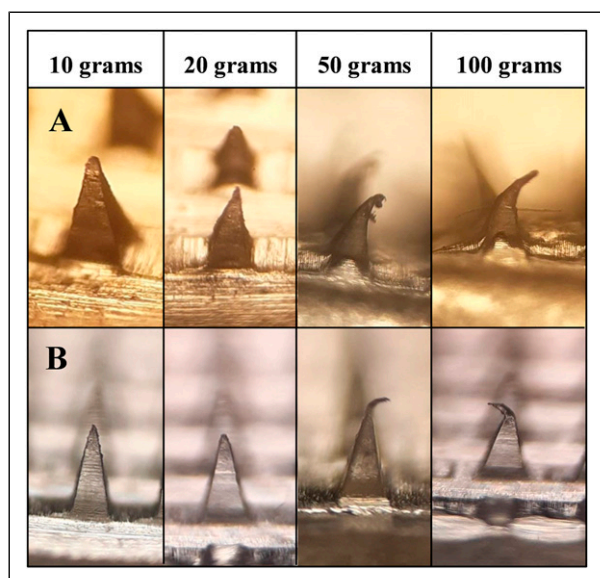
### Physical and Morphological Characterization of Microneedles

The microneedles, UN-1, were prepared with HPMC alone as a host material to evaluate the integrity of the array. The microneedles were neatly formed with complete structure. However, the polymeric solution (HPMC 8% w/w) could only be used as a needle solution and not as a baseplate. Hence, when PVA (15% w/w) was used as a baseplate material a complete microneedle array was obtained. Similarly, a combination of PVP (30%) with HPMC (8% w/w) in UN-2 resulted in a neatly formed microneedle array. The methylene blue dye was added in the aqueous polymeric material to assess the degree of uniformity and easier evaluation of the acral part of the microneedle under the microscope. The microscopic images revealed a sharp tip and strong microneedles from the aforementioned polymers and fabrication conditions as given in Table 2.

The dimension of the microneedle including (a) needle height, and (b) tip-diameter and angle were quantified using Image J software. In each case, the accuracy and repeatability in geometric parameters were statistically categorized for average and standard deviation by taking the measurements from (a) within the same array, (b) between different arrays in the same mold, and (c) between microneedles prepared in a different mold. Increased fluidity of HPMC-based microneedles (UN-1) yielded a significantly reduced apex angle ( $P < .05$ ) in comparison to the HPMC (8% w/w)-PVP (30% w/w) composite that had increased viscosity as shown in Table 2.

**Table 2.** Microscopic Images of Methylene Blue Containing Self-Dissolving Microneedle and their Dimensions.

Formulation code	Top View Images (40x)	Tip Diameter ( $\mu$ m)	Tip Angle <sup>o</sup>	Height ( $\mu$ m)	Deviation from Actual Height (%)
UN-1		15.71 ± 3.24	28.68 ± .34	598.11 ± 1.55	.32 ± .26
UN-2		20.41 ± 2.03	32.37 ± 1.51	599.32 ± .97	.11 ± .16



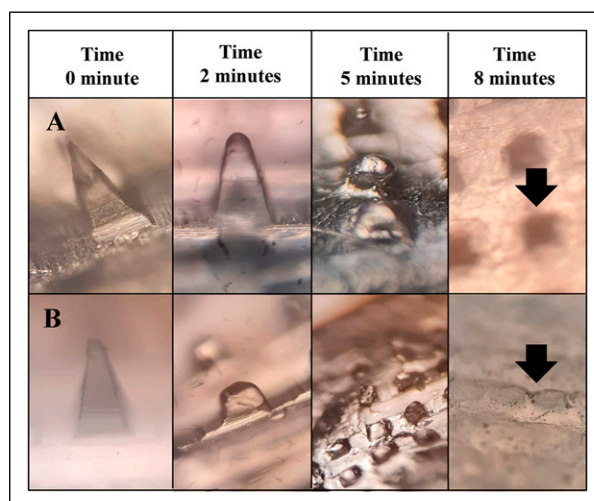
**Figure 3.** Mechanical strength and tip bending of self-dissolving microneedle under different weights.

Although the presence of PVP (30% w/w) with HPMC (8% w/w) in UN-2 increased the tip angle, the results were not statistically different ( $P > .05$ ). However, despite having different tip diameters ( $\mu\text{m}$ ), the heights of the microneedles were not significantly different ( $P > .05$ ).

### Mechanical Strength Test of Dissolving Microneedles

The ability of the microneedle to be inserted into the skin requires efficient mechanical properties. Polymeric microneedles require special attention for integrated mechanical strength in terms of polymer type and concentration as it has a direct relation with the skin insertion capacity and can influence storage settings.<sup>37</sup> Our studied polymers, at specific concentrations, showed that the microneedles could be designed with sufficient strength to endure a weight of up to 50–100 g. The mechanical integrity of various formulations under different weights is given in Figure 3. It was evident from the microscopic analysis that most of the needles started to bend after 50 g of weight was placed on the tips of an array. The deformation extended to a greater degree when 100 g weight was used.

When the compressed microprojections were analyzed under a light microscope, three distinct failure modes could be observed to characterize the behavior of mechanical strength as defined by Rapheal et al (2016), including (a) failure in bending of the tip, (b) tip failure due to abrupt brittleness, and (c) failure due to bulking.<sup>18</sup> In failure due to buckling, the lower part of the microprojection also bends plastically along with the tip. The microneedle UN-1 showed such deformation behavior as seen in Figure 3. This depicts ductile characteristics of the material that impose enough rigidity to resist the primary bending.<sup>18</sup> Failure in bending of the tip was observed



**Figure 4.** Microneedle insertion in Parafilm® for (A) UN-1, and (B) UN-2. A1–A3 and B1–B3 represent Parafilm® layers. The digital photographs represent microneedle geometry after insertion.

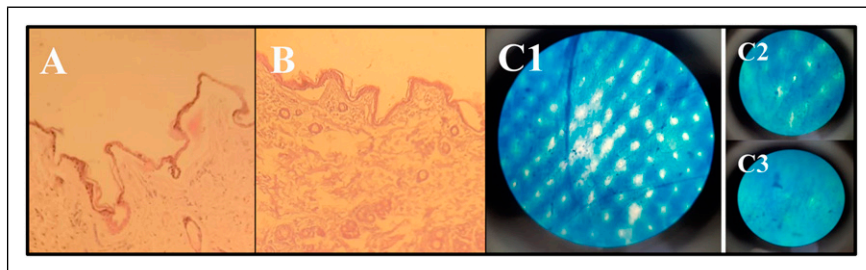
in UN-2 where the top half of the needle was deflected as shown in Figure 3. The deflection occurred due to the small initial bending of the microtip that continued to the plastic failure without evident bending of the shaft. These formulations had a composite mixture of polymers which signifies that a mixture of polymers adds strength to the needle structure. It is in good agreement with previous studies that verify that the combination of polymers forms microneedles with good mechanical properties in comparison to the individual polymer.<sup>38,39</sup>

### Insertion Depth of Dissolving Microneedle in Parafilm® M

A viscoelastic sheet, Parafilm® M, was used to predict the puncturing depth of the microneedle in an in vivo setup. Parafilm® M artificial membrane, folded in eight sheets, is often utilized to mimic as a full-thickness skin model for TDDS studies.<sup>15</sup> Figure 4 represents the number of holes punctured in the sheet after microneedle insertion where UN-1 was able to pierce through the third sheet more efficiently as compared to UN-2.

Furthermore, the thumb pressure moved a few microprojections to the fourth layer (~30 holes were visible in case of UN-1), but as they were less than 20% of the total microtips, the image was excluded.<sup>15</sup> This result is in good agreement with our previous data in which HPMC (8% w/w; UN-1) microneedles indicated sharper tips as compared to HPMC (8% w/w)-PVP (30% w/w) combination (UN-2). The length of the microneedles after insertion into the Parafilm® M is shown in Figure 4 that verifies the mechanical integrity of microneedles under stress conditions. The pores created in the Parafilm® layers indicate the uniformity of the needles, whereas the indentation area (seen in UN-2, Layer 2) suggests





**Figure 5.** Ex vivo polymer dissolution of self-dissolving microneedles (A) UN-1 and (B) UN-2.

that only a certain portion of micro-tip could penetrate the viscoelastic sheet. Based on the depth of the Parafilm® M (123.75–237.5  $\mu\text{m}$ ), it can be reasonably concluded that the formulated microneedles could bypass the stratum corneum (10–15  $\mu\text{m}$  thickness) and the viable epidermis (50–100  $\mu\text{m}$  thickness) to reach the superficial layer of the dermis. Most importantly, these microneedles would be able to create microchannels near the basal membrane (120–150  $\mu\text{m}$ ) where the herpes virus resides. The formation of these micropores in vitro can therefore predict the percutaneous delivery of the drug into the deeper sites and systematically.<sup>40</sup> Hence, the results signified the possible skin pre-treatment with UN-1 for subsequent administration of topical lyophilized wafer.

#### Ex vivo Polymer Dissolution in Excised Skin Model

The microscopic images of UN-1 and UN-2 in Figures 5A and 5B show the polymer dissolution profile of microneedles at different time intervals. Following insertion and removal from the skin after a predefined time, the tip of the microneedle was round and smooth in each case. The height of the needles decreased within 2 minutes in comparison to an otherwise sharp tip of the microneedle before skin insertion. There was no evidence of an instant buckling or breakage of the needles that confirmed the initiation of tip dissolution that progressed toward the shaft. The rounded needles demonstrated gradual dissolution as time progressed and dissolved within 10 minutes of the study.<sup>41</sup> Post-application, small stumps remained on the surface of the baseplate that indicated complete dissolution of the microprojections. The predicament of polymer dissolution is often connected with the water sorption capacity and hygroscopicity of the microneedle matrix. Generally, the hygroscopicity of the polymer mainly depends upon 2 factors, namely, (a) the presence of hydrophilic groups and (b) crystallinity of the polymer. If the polymer possesses lower crystallinity and more hydrophilic groups, then it would tend to have better moisture sorption property from the microenvironment and hence more hygroscopicity. The dissolving microneedles made of water-soluble polysaccharides such as HPMC contain abundant hydrophilic groups (like carboxyl groups and a hydroxyl group) which endow them with excellent solubility characteristics. Hence, polysaccharide-based microneedles can dissolve in the skin within a matter of

minutes. Polyvinyl pyrrolidone is often used in the microneedle due to its dual role as an additive: (a) increasing the affinity of a matrix to water and (b) acting as a pore-forming agent to improve dissolution profile.<sup>42</sup>

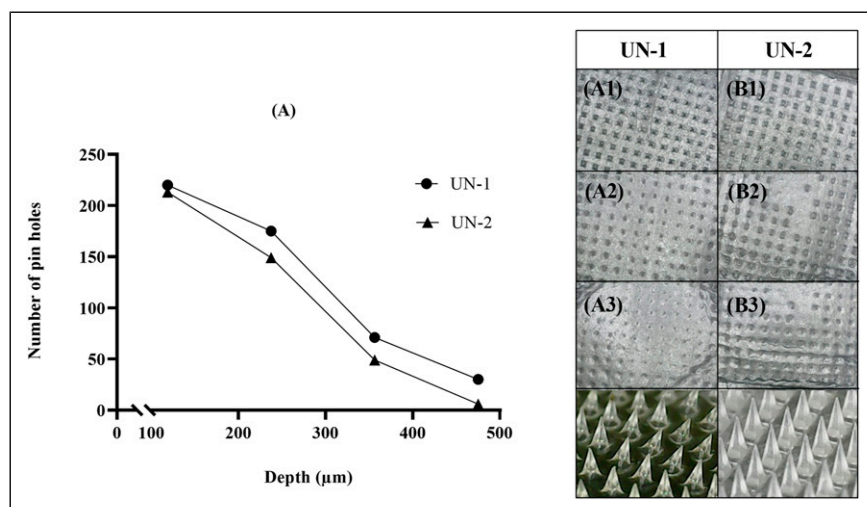
#### Skin Insertion Studies on Rabbit Skin and Staining

Regarding the piercing properties, Figures 6A and 6B depict the histological sections of the rabbit skin after microneedle insertion. The microneedle array always requires a certain pressure to get inserted into the skin, whether it be in the form of thumb pressure or an applicator. To exert a similar amount of pressure, the microneedles were inserted by one experimenter to reduce data biasness.<sup>19</sup> As evident, no dermal breaches were observed in this study. As the pain receptors are concentrated within the dermal layer, it is safe to claim that the designed microneedles will not cause any pain sensation.<sup>43</sup>

Effective and reproducible microneedle-drug delivery in the clinical setup depends exclusively on the predictable and reliable skin penetration efficiency and duration of pore sustenance. Methylene blue has been extensively adapted by researchers for the staining of skin after microneedle piercing due to its ability to effectively mark the damaged pores of the stratum corneum. As the holes developed in the skin are hydrophilic, the water-soluble dye can easily accumulate in the pores for *en face* visualization. Additionally, methylene blue has a high affinity for the proteins, so none of it can be found in the deeper skin layers. Therefore, the application of dye after piercing made the non-visible pores detectable as seen in Figure 6C.<sup>44</sup> As the sustenance of the micropore is of prime importance to allow the passage of acyclovir from the baseplate, the skin was monitored for 12 hours to analyze the resealing of micropores. As seen in Figure 6 (C1–C3), the number of micropores decreased as time progressed and almost diminished after 12 hours. Since methylene blue was not the real drug, it could still be used as a reliable stain for reasonable interpretation of drug distribution and resealing in microporated skin.

#### Characterization of Acyclovir Powder Suspension

Many iterations of the acyclovir lyophilized wafer were formulated to optimize the drug and excipient concentration within each unit of the drug reservoir (formulation code



**Figure 6.** Histological staining of (A) UN-1 and (B) UN-2. (C) Light microscopic image representing the distribution of methylene blue after puncturing of the skin with self-dissolving microneedle. The image also represents the successful piercing of skin (C1) immediately after microneedle insertion, and skin resealing (C2) after 2 hours, and (C3) after 12 hours.

F1–F4). Here, gelatin was used as a matrix-forming polymer due to its reported biocompatibility, biodegradability, bio-adhesive, and hydrophilic properties. Gelatin can form physical crosslinks that break at body temperature.<sup>45</sup> The addition of sodium chloride provided additional structural integrity to the drug reservoir.<sup>11</sup> Mannitol was added as a lyoprotector to prevent structural collapse during the freeze-drying process.<sup>46</sup> Production at laboratory scale allowed mixing of material by brief homogenization (60 seconds) followed by ultrasonication for 60 minutes. Visually, the powder solution was white due to the uniform distribution of ingredients during ultrasonication.

The formulations F1–F4 were placed in a bench-top freeze dryer to remove the water from the pre-frozen matrix by vacuum sublimation (formulation code: LW-1 to LW-4). After lyophilization, the drug powder showed a different pattern of homogeneity and sedimentation. The formulation LW-1 was sticky and did not form an adequate porous structure for easier scrapping. The nonhomogeneous powders (LW-3 and LW-4) had a clear distinct separation of translucent gelatin that was distinguishable in an otherwise white set of ingredients. Lead formulation (formulation code: LW-2) that appeared as a uniform and homogenous powder was subsequently selected to be taken forward for industrial-scale manufacturing. LW-2 contained acyclovir (40% w/w; equivalent to 200 mg of drug), gelatin (10% w/w), mannitol (5% w/w), and sodium chloride (5% w/w).

Freeze-dried wafers have low water content that prevents microbial growth in the formulation. Further still, to prevent such contamination during the manufacturing process, we prepared the wafer under sterilized conditions. For this, the lead formulation LW-2 was assembled in a glass vial at the end of a freeze-drying cycle in an industrial-scale automated freeze-drying chamber (LYO-10.0-CIP-SIP, Tofflon, China). As the freezing cycle controls the porosity and surface

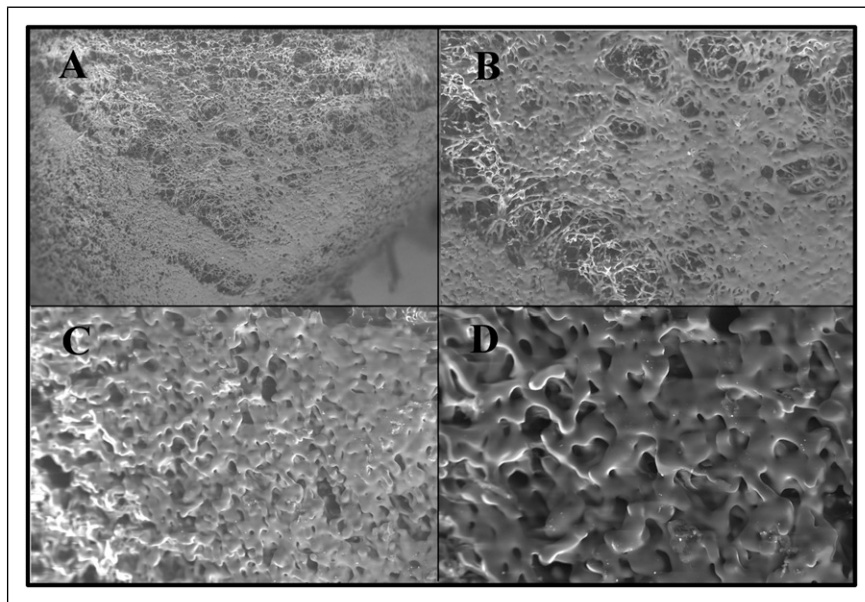
topology of wafer, therefore, the thermal procedure, target temperature, and the rate were entered in advance as represented in Figure 1. After solidification through freezing, the product goes into a deep vacuum. Here, the moisture removal from the frozen specimen occurs in two steps: primary drying (free solvent removal) and secondary drying (bound solvent removal). Primary drying usually has a longer duration as the bulk water sublimates at lower temperatures and larger amounts as compared to the bound water.<sup>47</sup> By the end of the lyophilization cycles, a white crystalline wafer was formed in the transparent glass vial sealed with an aluminum flip. This type of packaging also protects the fragile lyophilized wafer from physical stress and humidity.

#### *Physical Characteristics and Content Uniformity in Acyclovir-Loaded Topical Lyophilized Wafer*

The physicochemical properties of wafer were assessed, including weight variation, diameter, thickness, and percentage drug recovery. According to the manufacturing method adopted, the diameter of the porous wafer was  $13 \pm .24$ , whereas the thickness was quantified at  $12 \pm .15$ . The weight of the wafer was  $304.02 \pm 1.32$  mg. As per USP-NF criteria, the weight of the wafer complied with the specification of  $\pm 7.5\%$  deviation limit. The lyophilized wafer contained  $200.03 \pm .67$  mg of acyclovir mainly because of the automated filling system. The average percentage recovery of acyclovir from the drug reservoir was  $100.01 \pm .89\%$ .

#### *Scanning Electron Microscopy Analysis of Acyclovir Containing Lyophilized Wafer*

Scanning electron microscopy investigation showed that the lyophilized wafer of acyclovir was highly porous in



**Figure 7.** SEM photographs of the top surface of the lyophilized wafer at (A)  $\times 100$  magnification, (B)  $\times 250$  magnification, (C)  $\times 500$  magnification, and (D)  $\times 1000$  magnification.

morphology. Both the top and the sliced portion of the wafer was analyzed at different magnification as seen in Figure 7. As evident from the images, the top part of the wafer was less porous as compared to the bottom part. Such differences in the surface characteristics can have an impact on the physico-chemical properties including hardness, adhesion, and water sorption characteristics as previously reported in various works of literature.<sup>25,48</sup> The wafer consisted of large, uniform, and circular-shaped pores that were surrounded by a network of polymeric strands.<sup>25</sup> The results supported the claim of rapid hydration of lyophilized wafers when placed on the skin, section 4.5.3.2, due to the porous structure of the lyophilizate.

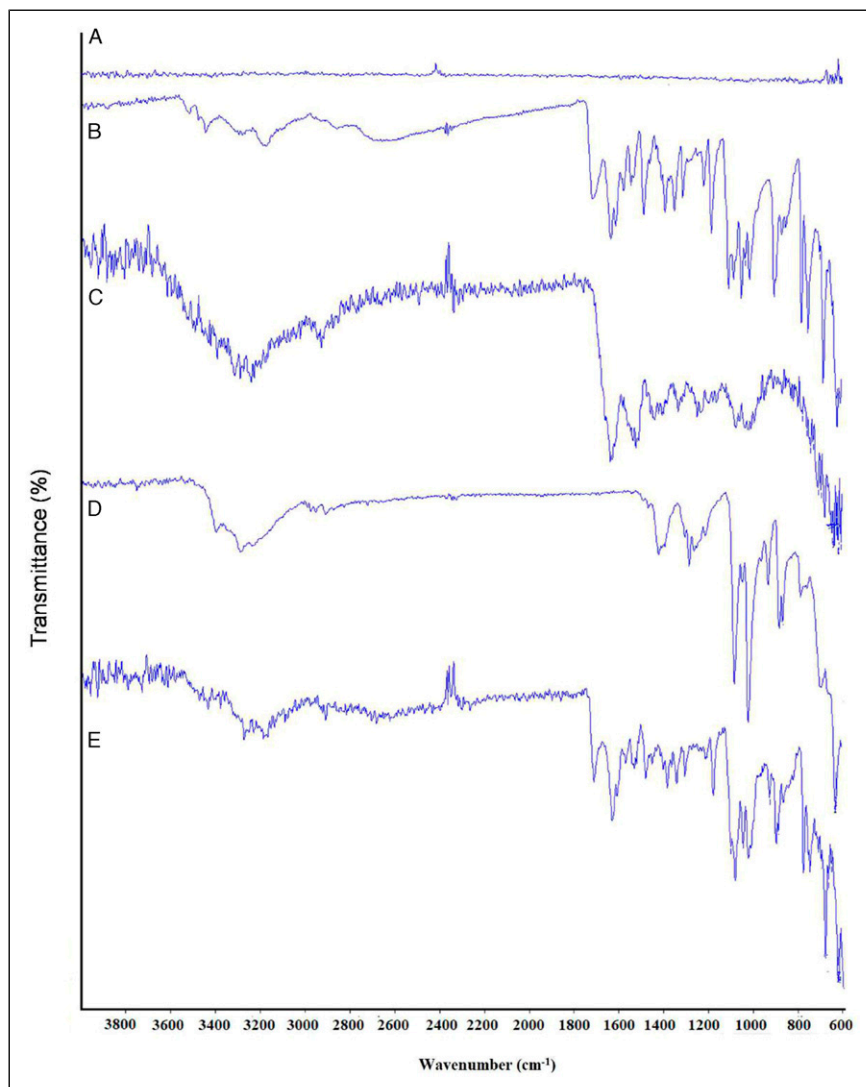
#### *Fourier Transform Infrared Spectroscopy of Acyclovir Containing Lyophilized Wafer*

Some major bands in FTIR spectra of pure acyclovir were evident at  $3436.25\text{ cm}^{-1}$ ,  $3176.45\text{ cm}^{-1}$ ,  $1706.97\text{ cm}^{-1}$ , and  $1626.50\text{ cm}^{-1}$  that corresponded to an amine group (-NH) stretching vibration, -OH stretching vibration, amide group (C=O) stretching, and -NH bending, respectively, as shown in Figure 8.<sup>49</sup> Fourier transform infrared spectroscopy spectra of gelatin showed the major peaks in the amide region. The vibration peak at the wavenumber of  $1634.16\text{ cm}^{-1}$  corresponded to amide I,  $1533.11\text{ cm}^{-1}$  to amide II, and  $1246.35\text{ cm}^{-1}$  to amide III. The amide I vibration mode was attributed to the C=O stretching vibration contributed by the amine group (-CN) stretch, nitrile group (-CCN) deformation, and -NH bending (in-plane). The amide II vibration modes were observed due to the out-of-phase coupled CN stretch and in-plane NH deformation of the peptide group. Alternatively,

the amide III mode represented the C-N stretching and NH deformation from amide linkage. This was coupled with a wagging vibration from  $-\text{CH}_2$  present in the peptide group.<sup>50</sup> The characteristic absorption peaks of mannitol were obtained at  $3405.63\text{ cm}^{-1}$ ,  $2946.52\text{ cm}^{-1}$ , and  $1077.64\text{ cm}^{-1}$  that indicated -OH stretching, -CH stretching, and -CO stretching, respectively.<sup>51</sup> The spectra of drug-loaded powder showed a superposition of each component that indicated that there was no interaction between the drug and other excipients. Although some of the peaks overlapped due to the similar chemical moieties, the characteristic peaks corresponding to specific moieties were similar.

#### *Differential Scanning Calorimetry Analysis of Self-Dissolving Microneedle and Topical Lyophilized Wafer Mixture*

The DSC thermogram of HPMC showed a broad endothermic peak, whereas the exothermic peak started at  $208.74^\circ\text{C}$ <sup>52</sup> (Figure not shown). The enthalpy relaxation of HPMC was very small and thus hardly distinguished. However, this should not be considered incorrect since the method has a strong dependency on the degree of crystallinity and molecular mass.<sup>53</sup> For more accurate glass transitional behavior, McPhillips et al (1999) have recommended the use of modulated-temperature differential scanning calorimetry (MTDSC) instead of conventional DSC to detect transitions in HPMC that involves small changes in heat capacity.<sup>54</sup> In the case of PVP, the first endothermic peak appeared at  $72.16^\circ\text{C}$  which was attributed to the glass transition process associated with an enthalpy of  $252.89\text{ J/g}$  and extended from  $41.12^\circ\text{C}$  to

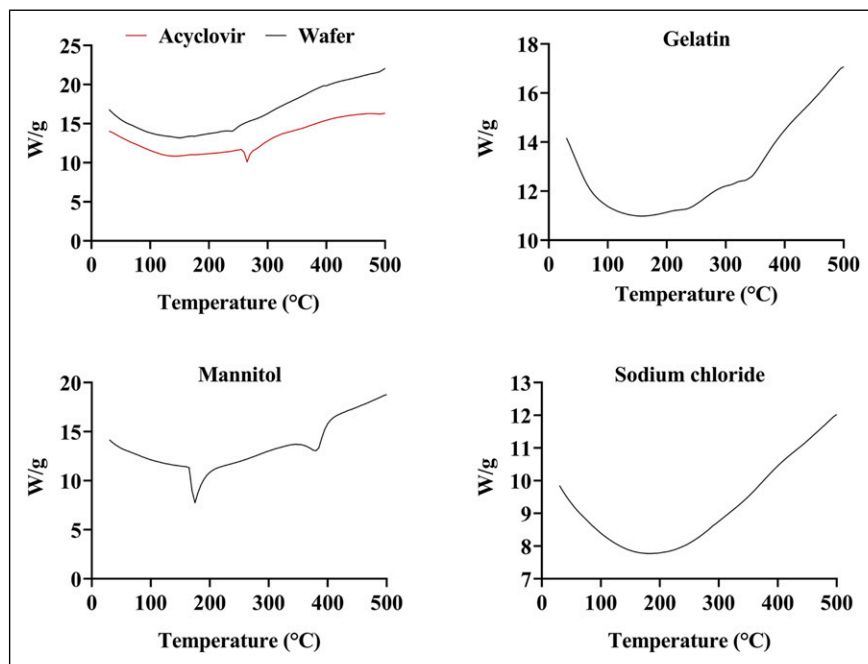


**Figure 8.** FTIR of (A) sodium chloride, (B) acyclovir, (C) gelatin, (D) mannitol, and (E) US-1.

approximately 124°C. The extended broad peak probably included another small one at approximately 100°C due to the removal of water entrapped in the polymer network. In addition to the endothermic peak at 72.16°C, the sample showed an additional deep endothermic peak at 403.14°C which indicated the thermal decomposition process that was associated with an enthalpy of 295.05 J/g.<sup>55</sup> The physical mixture of the polymers, HPMC and PVP, showed a similar thermal diagram to the individual polymers, without the appearance of a new thermal peak. The enthalpy of the physical mixture also decreased drastically from 252.89 J/g to 157.31 J/g.

The DSC thermograms of acyclovir showed a sharper endothermic peak at 263.57°C that corresponded to the transition melting of the drug with an associated enthalpy of 104.88 J/g<sup>56</sup> as shown in Figure 9. The DSC thermograms of gelatin powder showed a broad region in the thermogram trace, starting from 29.10°C to above 150°C with a minute

calorimetric enthalpy. This endothermic region was associated with the glass transition temperature of gelatin due to the transition of a triple helix to random coil and water loss. In addition, a weak transition was observed at almost 214–240°C which might be due to the breakage of peptide bonds leading to polymer degradation. A slight endothermic peak also appeared near 320.91°C. These findings were in agreement with previous reports of various authors.<sup>57,58</sup> In the thermogram of mannitol, a sharp endothermic peak was observed at 172.99°C with an enthalpy of 298.16 J/g. The second endothermic was evident at a peak temperature of 381.78°C, indicating the decomposition process of the sample as confirmed by Arikotla et al (2014).<sup>59</sup> In the case of the sodium chloride thermogram, the dip in the peak might be attributed to the water loss as seen in Figure 9. Otherwise, according to reported literature, the melting of sodium chloride does not start before the onset temperature of 801°C.<sup>60</sup> As the present studies were



**Figure 9.** DSC thermograms of drug, polymers, and lyophilized wafer of acyclovir.

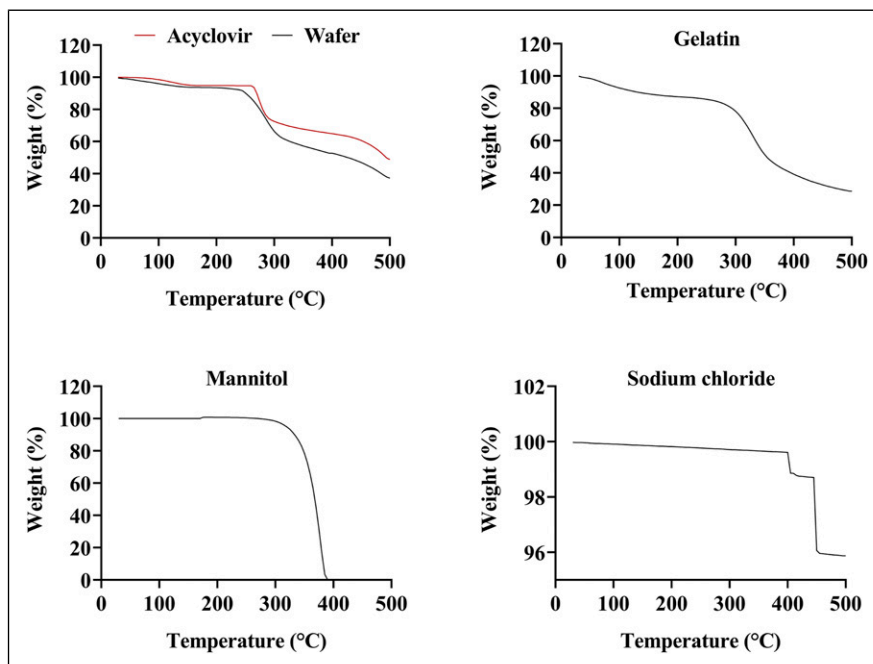
conducted at a maximum temperature of 500°C, hence the sharp endothermic peak corresponding to the melting of the compound was not visible. In the lyophilized powder of Acyclovir, an endothermic peak was visible at 221.81°C which may be attributed to the breakage of the peptide bonds present in the gelatin powder. Otherwise, only minute peaks were observed near the melting range of mannitol as evident in Figure 9. Most importantly, the drug-loaded wafer did not show any characteristic endothermic peak for acyclovir melting transition which suggests that the drug was molecularly dispersed within the wafer matrix as an amorphous. A similar finding was reported by Avachat et al (2018) which reported uniform dispersion of drug in the lyophilized liposomal wafer.<sup>61</sup>

#### **Thermogravimetric Analysis of Self-Dissolving Microneedle and Topical Lyophilized Wafer Mixture**

Thermogravimetric of HPMC displayed a gradual weight loss of about 3.9% before 100°C corresponding to the moisture loss from the polymer (Figure not shown). A single-step degradation accelerated in the temperature range of 239.07–398.57°C with a weight loss of 79.89%. Hydroxypropyl methylcellulose often displays higher thermal stability due to the presence of linear and strongly hydrogen-bonded molecules as reported by Swamy et al (2009).<sup>62</sup> According to TGA thermograms of PVP, the polymer showed two decomposition steps. The first step occurred at a temperature range of 32.53–196°C with a weight loss of around 17% that corresponded to a combined weight loss of residual moisture and low molecular weight oligomers. The second step occurred in

the temperature range of 344.41–484.09°C and displayed a total weight loss of 64.59% which represented the complete decomposition of the polymer.<sup>63,64</sup> The TGA analysis of HPMC with PVP blend displayed 2 decomposition states. The first stage was observed between the temperature range of 32.06–146.44°C that was related to the moisture evaporation and residual weight of low molecular weight oligomers of PVP. The first step displayed a gradual weight loss of 11.94%. The second decomposition state started near 250°C that continued to approximately 488.39°C. During this transition, first, the melting of HPMC occurred with a further weight loss of 45.84% near 412.84°C. This was followed by the chemical decomposition of PVP that showed a rapid weight loss of 33.63% to 488.39°C. A similar finding was reported by Derya (2020) that confirmed such transition changes for the HPMC-PVP blend.<sup>65</sup>

The obtained TGA graph of Acyclovir showed a thermal event near 263.57°C that indicated the melting point of the drug as displayed in Figure 10. In addition, only a narrow dip was noticed near 100°C, corresponding to 1.5% of the total weight loss that might be attributed to the removal of water vapors. Thus, based on the combined results of TGA and DSC, it was established that acyclovir was thermally stable up to the melting point. Near 440.2°C, a major weight loss was observed that indicated the start of acyclovir decomposition due to the cleavage and elimination of the alcoholic-etheric side chains from the drug structure.<sup>66</sup> Mannitol displayed a rapid mass loss after 295°C that could be attributed to the decomposition of the polymer with a total weight loss of 98% till 500°C as indicated in Figure 10.<sup>67</sup> Due to the higher molecular stability of sodium chloride, the TGA curve of the



**Figure 10.** TGA thermograms of drug, polymers, and lyophilized wafer of acyclovir.

salt only showed a negligible weight loss of around 4% during the thermal analysis. In addition, a weight loss of .13% was observed before 140°C, which eliminates the possibility to hydrate or solvate formation of the salt crystals. The minute weight loss between the temperature range of 400–450°C might be due to the sublimation of the solids.<sup>68</sup> Otherwise, as discussed in DSC results, the melting range of sodium chloride occurs near 800.1°C.

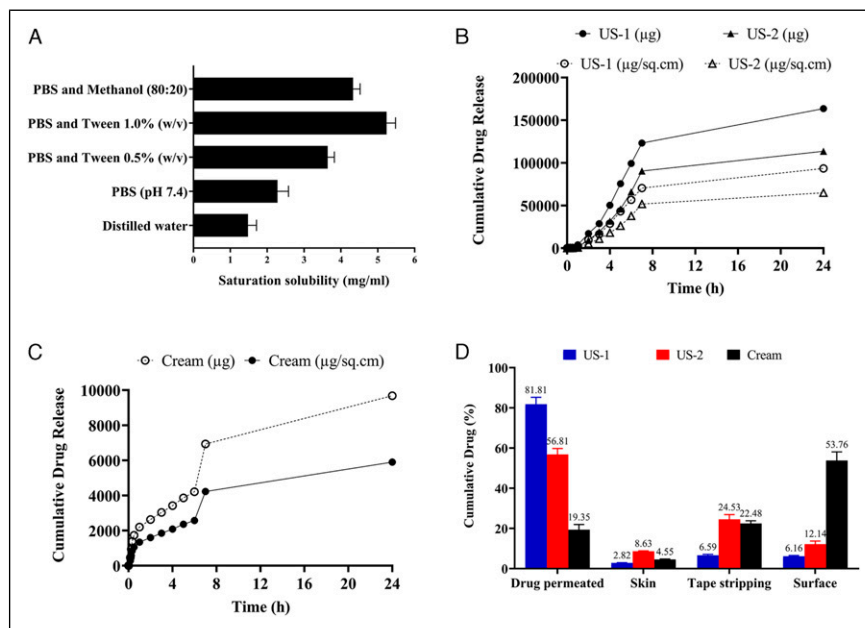
The TGA curve of a lyophilized wafer, shown in Figure 10, depicted a weight loss of around 6% in the temperature range of 22.33°C to 143°C. Based on the previous discussion it might be expected that this weight loss referred to water vaporization. However, considering the first decomposition stage of gelatin, this temperature range also included the decomposition weight loss of gelatin due to helix-coil transition. The weight loss till 100°C was approximately 4%. Considering the low molecular weight of water in comparison to gelatin, it was expected that the amount of moisture present in the lyophilized wafer could be considered to be in an appropriate low range. It also needs to be considered here that the equilibrium moisture content of the lyophilized wafer is also a reflection of environmental conditions. As discussed in detail by Mathews et al (2008), low water content is obtained in the final stages of a freeze-drying cycle of lyophilization, but it is quickly increased by fast equilibration at laboratory conditions.<sup>69</sup> The obtained moisture levels were comparable to other reported studies by Kim et al (2009),<sup>70</sup> Kianfar et al (2014),<sup>71</sup> and Farias and Boateng (2018).<sup>72</sup> Water content after lyophilization is typically expected to be in a range of .5–3%. Lower water content reduces molecular mobility which ensures shelf-life of the formulation by avoiding earlier

hydration of the drug moiety. High-residual content may act as a seed to accelerate the crystallization process which might lead to polymorphism within the system. This eventually increases the system instability.<sup>71</sup> Further, due to the intended topical application of the wafer on the skin, an optimum state of hydration implies the wafer to function efficiently under compression induced by occlusive dressing Tegaderm™.<sup>25</sup> Hence, the present system was considered thermally stable in the current stages of primary and secondary drying. The second curve in the TGA of US-1 was obtained at the 230–330°C range with a recorded weight loss of 31.68% that signified the decomposition phase of gelatin. The weight loss corresponded well with that observed in the TGA curve of gelatin which ensured that no thermal decomposition of the drug was evident during the process.

### *Selection of Receptor Media for the Maintenance of Sink Conditions*

For the skin permeation studies, the recommended receptor media are the aqueous buffers with appropriate pH related to the physiological environment. The use of additives in the testing media is often necessary in some cases to increase the solubility of the drug. The final composition and volume of the media must assure sink conditions such that the drug concentration must not reach values > 10% of its saturation.<sup>73</sup>

Based on testing, the maximum solubility of acyclovir was obtained in PBS (pH 7.4) containing 1.0% w/v Tween 80 (5.24 mg/mL), followed by methanol (80:20) mixture (4.33 mg/mL), and PBS with .5% w/v Tween 80 (3.64 mg/mL) as depicted in Figure 11A. The lower solubility was obtained



**Figure 11.** (A) Saturation solubility of acyclovir in different solvents and buffer conditions. *Ex vivo* cumulative drug release of (B) US-1 and US-2 and (C) topical marketed cream of acyclovir. (D) Percentage drug permeated and drug retention in skin, stratum corneum (tape stripping method), and surface of skin.

in PBS (2.28 mg/mL) and distilled water (1.48 mg/mL). Hence, PBS pH 7.4 with Tween 80 (1.0% w/v) was used for further *ex vivo* permeation studies as a receptor fluid. Tween 80 was selected as the surfactant of choice due to its established efficacy in improving the solubility of drugs during dissolution studies.<sup>74</sup> The solubility is often enhanced by the said surfactant due to the reduction in the interfacial tension between the solid–liquid interfaces that increases the wetting of the drug to a higher degree.<sup>75,76</sup> Although acyclovir had higher solubility in Tween 80 in comparison to the other additives, its increased viscosity and foaming restricted its use at higher concentrations.<sup>76</sup> In addition, when used in concentration much beyond the critical micelle concentration, Tween 80 may reduce and hamper the dissolution rate constant by lowering the diffusion rate of the micelle-solubilized entity.<sup>76</sup> Also, a dissolution medium containing surfactants can better simulate the *in vivo* conditions as compared to the organic solvents or other non-physiological agents. This aids in evaluating the quality of the drug as a future predicament for *in vivo* settings.<sup>77</sup>

The *ex vivo* experimental protocol adapted for skin pre-treatment and permeation studies of drug reservoir is diagrammatically represented in Figure 11A. As seen in the image, the self-dissolving microneedle array (x3 microneedles fixed on surgical adhesive tape) was used to puncture the stratum corneum with a constant downward thumb pressure for 30 seconds. Afterward, the array was left in the skin for 5 minutes to ensure polymer dissolution and micropore sustenance. The blank baseplate was removed after the stated time or simply wiped with a wet cloth. Later, the perforated skin

was placed on the donor compartment of the Franz diffusion cell, and the topical wafer was placed carefully on the punctured area. The donor compartment was clamped securely and sealed with Parafilm<sup>®</sup> M to prevent medium evaporation.

Figures 11B and 11C represent the *ex-vivo* permeation profile of acyclovir from the topical lyophilized wafer across the microneedle-treated rabbit skin and commercial cream formulation. US-1 represents topical wafer placed on UN-1 treated skin, and US-2 refers to application of lyophilized wafer on UN-2 treated skin. The data demonstrate that polymeric microneedle-treated skin could deliver a higher dose of a drug through the animal skin and that the delivery efficiency was dependent on the polymers used for initial microneedle-skin treatment.

Figure 11D depicts that the microneedle-treated skin permitted the permeation of 81.81% and 56.81% ( $P < .05$ ) of the drug across the skin through topical lyophilized wafer over 24 hours from US-1 and US-2, respectively. At the same time marketed formulation passively delivered only 19.24% of the drug across the skin. As depicted in Figure 11D, a low percentage of the drug was retained on the skin surface after 24 hours from the lyophilized wafer. This signifies the sustenance of micropores for a longer time as discussed in micropore sustenance previously. The results also display that acyclovir was retained in the stratum corneum and skin (site of HSV infection) for a longer duration. Hence, the proposed system could be used both for local delivery and systemic drug availability, depending upon the polymer selected for microneedle fabrication. As discussed previously, passive

**Table 3.** Ex-vivo Permeation Analysis of Topical Lyophilized Wafer on Self-Dissolving Microneedle Pre-Treated Skin (US-1 and US-2) with Marketed Cream Formulation (Passive Delivery).

Ex vivo Parameter	US-1	US-2	Cream
Q ( $\mu\text{g}$ ) at 24 hours	163 614.35 $\pm$ 48.28	113 614.21 $\pm$ 34.46	9676.75 $\pm$ 12.24
Q ( $\mu\text{g}/\text{sq.cm}$ ) at 24 hours	93 493.91 $\pm$ 294.38	64 922.40 $\pm$ 364.60	5900.46 $\pm$ 103.87
Q (%) at 24 hours	81.81%	56.81%	19.24%
Steady-state flux (Jss) ( $\mu\text{g}/\text{sq.cm.h}$ )	4275.40	2987.9	225.57
Permeation enhancement ratio (PER)	18.95	13.25	–
Lag time (h)	1.82	1.59	4.68
Q in skin ( $\mu\text{g}$ )	3219.89 $\pm$ 126.74	9866.00 $\pm$ 286.15	1386.79 $\pm$ 62.62
Q in stratum corneum ( $\mu\text{g}$ )	7530.75 $\pm$ 109.63	28 034.75 $\pm$ 198.34	6891.40 $\pm$ 145.30
Q remaining in baseplate/surface of the skin ( $\mu\text{g}$ )	7044.20 $\pm$ 59.85	13 878.04 $\pm$ 241.68	16 482.51 $\pm$ 63.08

delivery of acyclovir displayed reduced drug permeation and a large percentage of acyclovir retained on the skin surface.

As evident from the results given in Table 3, US-1 provided better flux of drug across UN-1 pre-treated skin as compared to the same formulation across UN-2 pre-treated skin (US-2). These results were in good agreement with the skin insertion analysis and Parafilm<sup>®</sup> M insertion depth analysis where UN-1 provided greater depth as compared to UN-2. The enhancement in permeation across the microperforated skin was also greater in the case of US-1. Contrary to that, passive delivery of Acyclovir across the excised skin provided the least flux in 24 hours, and most of the drug was retained on the skin surface, rather than permeate across it. This result was in true agreement with previous reports of Nair (2015) who demonstrated the concentration gradient of acyclovir to be the highest in stratum corneum, followed by viable dermis and dermis after topical application.<sup>78</sup> Our results confirm the fact that by-passing the stratum corneum to provide the drug directly near the dermis can greatly improve the drug availability in the skin layer and systematically. As discussed before, a crucial factor in transdermal technology is the lag time that is described as the time required for the drug to bypass the skin layers to reach the blood circulation. UN-2-treated skin depicted a lower lag time (US-2), although  $Q_{24}$  ( $\mu\text{g}/\text{sq.cm}$ ) was lower than UN-1-treated skin (US-1). The lag time was shortest for US-2 mainly due to the rapid dissolution of a polymer matrix containing PVP (30% w/w) in addition to HPMC (8% w/w). In addition, the shortest lag time of microneedle-treated skin might be due to the improved skin insertion depth achieved after the physical application of the microneedle. The micropores created in the stratum corneum and viable epidermis shortened the traveling distance of the drug and allowed the drug to diffusion into the dermal layer where the blood vessels reside. The lag times of US-1 and US-2 were significantly different from one another ( $P < .05$ ). In contrast, the control formulation depicted higher lag time mainly due to the hindrance experienced by the stratum corneum. The pre-treatment of skin with self-dissolving microneedles before topical application of wafer had dramatically increased the PER. In addition, US-1 also provided

improved enhancement in comparison to acyclovir-loaded ethosomal preparation reported by Alshehri et al (2021). In that study, acyclovir-based ethosomal gel provided 1.75 folds increase in enhancement ratio in an ex vivo setup as compared to the marketed cream formulation.<sup>79</sup>

Studies have reported that acyclovir inhibits 99% (ID<sub>99</sub>) of viral infection at an average concentration of 4.21  $\mu\text{g}/\text{ml}$ .<sup>10</sup> The proposed topical lyophilized wafer provided ~4.5–16 times higher skin concentration than the ID<sub>99</sub> reported. Therefore, these results suggest that a self-dissolving polymeric microneedle-assisted topical lyophilized wafer system would be efficacious against HVI existent in the skin layer and for systemic therapy. Based on the previous finding of Parnornpathomkul et al. (2018), pertinent to microneedle-assisted delivery of acyclovir, the authors reported a five-fold increase in ID<sub>99</sub>.<sup>10</sup> Hence, our system provided much better and quantifiable results.

Two aspects need to be considered here based on the current study; (a) drug retention is required near the basal membrane where the herpes virus usually resides, and (b) systemic acyclovir is required to provide the drug to site where the topical dosage form is otherwise hard to be retained, for example, near lips (cold sores due to HSV-1) or genital areas (genital herpes due to HSV-1 or HSV-2). In addition, systemic acyclovir would also be useful in complicated cases of HVI where herpes simplex encephalitis (HSE) occurs.<sup>80</sup> Based on these presumptions and result findings, US-3 was further taken for in vivo analysis to determine plasma drug concentration in an animal model.

### In Vivo Pharmacokinetic Analysis of Lyophilized Wafer of Self-Dissolving Microneedle Skin

The in vivo pharmacokinetic studies were done on albino rabbits to quantify the plasma concentration of acyclovir after topical administration of the wafer on self-dissolving microneedle-treated skin on hairless skin. The scheme adopted for in vivo pharmacokinetic studies is given in Figure 2B. Before the formation of a calibration curve, the drug and blank plasma were run discretely on the HPLC to



**Table 4.** Pharmacokinetic Parameters of Acyclovir after Topical Administration of Lyophilized Wafer on Self-Dissolving Microneedle Treated Skin (Formulation Code: US-1).

Parameter	Unit	Value
$t_{1/2k_a}$	h	3.50
$t_{1/2k_{10}}$	h	3.54
V/F	(mg)/(μg/ml)	8.60
CL/F	(mg)/(μg/ml)/h	1.68
Tmax	h	5.22
Cmax	μg/ml	2.58
AUC <sub>0-t</sub>	μg/ml* <sup>h</sup>	33.86
AUC <sub>0-∞</sub>	μg/ml* <sup>h</sup>	35.68
AUMC	μg/ml* <sup>h</sup> <sup>2</sup>	362.56
MRT	h	10.16

obtain their retention time on the chromatogram. Acyclovir retention on the chromatogram was obtained at 3.45 minutes, whereas the blank plasma gave a retention time of 3.30 minutes, respectively. Next, when the plasma was spiked with acyclovir, a slight shift in the retention time of plasma and drug was seen. The plasma retention time was detected at 2.94 minutes, while the drug gave a retention time of 3.43 minutes.

The calibration curve of pure acyclovir in animal blood plasma was constructed in the mobile phase comprising acetonitrile and 5mM ammonium acetate buffer pH 4.0 at 60:40 v/v ratios. Different dilutions of acyclovir were analyzed on HPLC, and their mean peak areas were recorded. The calibration curve was constructed between mean peak areas and nominal acyclovir concentrations that yielded a linear line equation of  $y = 647.07x + 2174.2$  with an  $R^2$  value of .9991. The results indicated that the AUC increased linearly with an increase in the concentration of acyclovir.

In the time course of the in vivo study, none of the rabbits showed any sign of ill health or adverse effect, neither as a result of self-dissolving microneedle insertion nor during the topical wafer administration. The assumptions made before the in vivo analysis included (a) the initial concentration of drug in the lyophilized wafer was 40 mg/kg, (b) a concentration of .0 μg/cm<sup>2</sup> existed on the skin at t = 0 minutes, and (c) complete wafer surface area was touching the skin once the wafer was affixed on the skin surface. The drug was detected in the animal plasma within 1 hour of US-1 administration that gradually reached the concentration of 3.97 μg/ml by the end of the seventh hour as seen in Table 4. This observation indicates the transport of acyclovir into the dermal area from the viable epidermis and stratum corneum, even after the closure of microchannels created by the self-dissolving microneedle. Afterward, the drug concentration declined by the end of the ninth hour which suggests the rapid clearance of the drug from the general circulation. The susceptibility of HSV-1 to acyclovir has been reported in the drug concentration range of .02–.90 μg/ml.<sup>81</sup> This demonstrated that the plasma level of acyclovir after a single administration of US-1 could be

maintained above the desired concentration for a longer time. This would particularly be more useful when serious cases are encountered, including HSE.<sup>80</sup> This data also ensured the availability of drugs near the basal membrane and within the skin layers for a prolonged time. The dermal location of the drug would be desirable to interfere with the latent HSV infection during repetitive administration and would inhibit human-to-human transmission by preventing the onset of disease.<sup>82</sup>

Based on pharmacokinetic parameter analysis, the Cmax was estimated to be 2.58 μg/ml at 5.22 hours (Tmax) as given in Table 4. The lyophilized wafer displayed an AUC<sub>0-∞</sub> of 35.68 μg/ml.h with an MRT of 10.16 hours. MRT in our study was significantly different from the MRT reported for oral acyclovir (2.07 h).<sup>81</sup> The AUC<sub>0-∞</sub> of 35.68 μg/ml.h obtained with US-3 was also better than the reported oral AUC<sub>0-∞</sub> of 28.74 μg/ml.h.<sup>81</sup> The in vivo permeation experiment showed that the cumulative permeation of acyclovir to systemic circulation decreased to large extent relative to the ex vivo permeation studies. The observation was possibly justified due to the difference in subcutaneous tissue fluid volume which varies excessively from the PBS (pH 7.4) present in the receiver compartment of the Franz diffusion cell. Two possible phenomena controlled wafer disintegration and drug release, namely, (a) thermo-responsive behavior of gelatin and (b) imbibition of skin moisture by the wafer. Gelatin is a biopolymer that is prepared by thermal denaturalization of collagen. As a gelling agent, it displays thermo-reversible properties, that is, at a lower temperature, it exists in a collagen-fold configuration that tends to form hydrogen bonds, while above 35°C, gelatin exists as a single molecule that is unable to develop interchain hydrogen bond. This gives the dosage form a ‘melting effect’ at body temperature which ultimately results in drug release.<sup>83</sup> Secondly, the polymer was hydrated due to the capillary forces of the pores (generated by self-dissolving microneedle pre-treatment) to imbibe moisture from the skin. Being a bioadhesive hydrophilic polymer, gelatin has a high tendency to absorb moisture that can subsequently lead to drug release patterns.<sup>45</sup>

### Accelerated Stability Testing

The stability testing of a microneedle patch and the lyophilized wafer was done under accelerated storage conditions following ICH and WHO guidelines. The preparations were stored at 40 ± 2°C, 75 ± 5% RH conditions for 168 days and assessed for different parameters at pre-defined intervals of 7, 28, 84, and 168 days.<sup>36</sup>

For the experimental test period, there was no loss in the physical integrity of the microneedles as shown in Table 5. No visible differences were found in microneedle arrays under 168 days’ storage conditions when compared to the reference source (Day 0). As for the acyclovir-lyophilized wafer, due to the complete seal integrity of the glass vial, no internal discoloration was observed. In addition, there was no visible change in the

**Table 5.** Physical Characteristics of Blank Self-Dissolving Microneedle UN-I (HPMC 8% w/w).

Parameter	Microneedle			Wafer	
	Polymer Distribution	Needle Deformation or Breakage	Contraction or Bending of the Baseplate	Color change	Drug content
0 Day	Uniform	None	None	None	100.10 ± .89
7th Day	Uniform	None	None	None	100.02 ± .75
28th Day	Uniform	None	None	None	99.67 ± .38
84th Day	Uniform	None	None	None	99.84 ± .46
168th Day	Uniform	None	None	None	99.59 ± .61

primary packaging or loss of its functionality during the stability testing under accelerated storage duration. With regard to the shape and color, individual wafers retained their circular shape and white color after 168 days. It was also noted during the testing period that the percentage of acyclovir in the lyophilized wafer remained consistent as given in Table 5 where the only negligible difference in drug content was observed. This resulted in a non-significant difference ( $P < .05$ ) in the acyclovir content (%) between Day 0 and Day 168.

## Conclusion

Being a commonly used antiviral drug, it has been widely suggested to adopt strategies that improve the bioavailability of acyclovir whilst reducing frequent dosing. Hence, it was established to explore self-dissolving microneedles to support the transdermal route of acyclovir for the provision of the drug near the basal membrane where the herpes virus resides in addition to the plasma concentration that might target other associated infected sites such as the brain. Additionally, the work presented the practical solution of overcoming the skin barrier function to provide a large dose of acyclovir across the skin by using topical lyophilized wafer on self-dissolving microneedle-treated skin. Researches have yielded significant evidence of using a lyophilized wafer with a hydrogel-based microneedle array. However, to date, these wafers have not been tested with a self-dissolving microneedle array. The use of such system can drastically reduce the lag time and provide large-dose acyclovir directly into the dermal layer.

Compared to multiple polymer concentration and/or combinations, microneedles prepared with HPMC (8% w/w) and HPMC (8% w/w)-PVP (30% w/w) provided the desired characteristics. The polymer shrinkage during manufacturing was sufficient enough to easily remove the microneedle from the mold whilst maintaining considerable height nearer to the desired height of 600  $\mu\text{m}$ . These microneedles possessed sufficient tip sharpness to cause piercing of the stratum corneum and rapidly dissolved in excised animal skin within 5 minutes. The microneedles displayed satisfactory depth, corresponding to 123.75–237.5  $\mu\text{m}$  when inserted in Parafilm M<sup>®</sup>. This reflected enough insertion of needles to reach the superficial layer of the dermis. Using such properties, the arrays were inserted

and retained in excised animal skin for 5 minutes to reversibly puncture the stratum corneum for the formation of microchannels through the epidermis. Subsequently, the topical lyophilized wafer was placed on microperforated skin. Due to the thermosensitive properties of gelatin, the hydration of polymer through microchannels led to the formation of gel that continued to become more mobile within 4 hours to achieve complete disintegration. In addition, mannitol and sodium chloride acted as hygroscopic agents to improve the disintegration rate of a lyophilized wafer. The wafer consisted of large, uniform, and circular-shaped pores that were surrounded by a network of polymeric strands as seen in SEM photographs. Additionally, the two dosage forms showed a thermally stable system as per DSC and TGA analysis. X-ray Diffraction (XRD) pattern of optimized drug-loaded microneedle and wafer showed a typical profile of amorphous material where sharp peaks of acyclovir crystal experienced reduced intensity. Based on ex vivo analysis on Franz diffusion cell, the data suggested that skin pre-treated with HPMC (8% w/w) –based microneedles allowed better cumulative drug release ( $\mu\text{g}/\text{sq. cm}$ ) and flux ( $\mu\text{g}/\text{sq. cm. h}$ ). The use of lyophilized wafer on pre-treated skin greatly improved the permeation rate compared to acyclovir-loaded dissolving microneedles and commercially available cream. Skin sampling revealed that lyophilizate provided ~4.5–16 times higher skin concentration than the ID<sub>99</sub> reported for acyclovir. Furthermore, the plasma level of acyclovir in albino rabbits after a single administration of wafer was maintained above the desired concentration for a longer period. The optimized microneedles and topical wafer maintained their physicochemical properties during accelerated stability studies.

## Declaration of Conflicting Interests

The author(s) declared no potential conflicts of interest with respect to the research, authorship, and/or publication of this article.

## Funding

The author(s) received no financial support for the research, authorship, and/or publication of this article.

## ORCID iD

Kashif Barkat  <https://orcid.org/0000-0003-4038-6035>

## References

1. Speck-Planche A, Cordeiro MNDS. Application of bioinformatics for the search of novel anti-viral therapies: Rational design of anti-herpes agents. *Curr Bioinf.* 2011;6(1):81-93.
2. Shin S, Kim TH, Jeong SW, et al. Development of a gastroretentive delivery system for acyclovir by 3D printing technology and its in vivo pharmacokinetic evaluation in Beagle dogs. *PLoS One.* 2019;14(5):e0216875.
3. Krasny HC, de Miranda P, Blum MR, Elion GB. Pharmacokinetics and bioavailability of acyclovir in the dog. *J Pharmacol Exp Therapeut.* 1981;216(2):281-288.
4. Ronald I, Shorr ABH, Nathan R. *A. Drugs for the Geriatric Patient.* Philadelphia, USA: W.B. Saunders; 2007:1-115.
5. Cortesi R, Esposito E. Acyclovir delivery systems. *Expet Opin Drug Deliv.* 2008;5(11):1217-1230.
6. Donalisio M, Leone F, Civra A, et al. Acyclovir-loaded chitosan nanospheres from nano-emulsion templating for the topical treatment of herpesviruses infections. *Pharmaceutics.* 2018;10(2):46.
7. Costa JSR, de Oliveira Cruvinel K, Oliveira-Nascimento L. A mini-review on drug delivery through wafer technology: Formulation and manufacturing of buccal and oral lyophilizates. *J Adv Res.* 2019;20:33-41.
8. Nguyen HX, Bozorg BD, Kim Y, et al. Poly (vinyl alcohol) microneedles: Fabrication, characterization, and application for transdermal drug delivery of doxorubicin. *Eur J Pharm Biopharm.* 2018;129:88-103.
9. Qian S, Chen Y, Gui S, Wang J, Zhou Y, Chen L. Enhanced penetration of sinomenine formulations following skin pretreatment with a polymer microneedle patch. *Lat Am J Pharm.* 2014;33(3):464-469.
10. Pamornpathomkul B, Ngawhirunpat T, Tekko IA, Vora L, McCarthy HO, Donnelly RF. Dissolving polymeric microneedle arrays for enhanced site-specific acyclovir delivery. *Eur J Pharmaceut Sci.* 2018;121:200-209.
11. Courtenay AJ, McAlister E, McCrudden MTC, et al. Hydrogel-forming microneedle arrays as a therapeutic option for transdermal esketamine delivery. *J Contr Release.* 2020;322:177-186. doi:10.1016/j.jconrel.2020.03.026.
12. McCrudden MTC, Alkilani AZ, Courtenay AJ, et al. Considerations in the sterile manufacture of polymeric microneedle arrays. *Drug delivery Translat Res.* 2015;5(1):3-14. doi:10.1007/s13346-014-0211-1.
13. McAlister E, Dutton B, Vora LK, et al. Directly compressed tablets: A novel drug-containing reservoir combined with hydrogel-forming microneedle arrays for transdermal drug delivery. *Adv Healthcare Mater.* 2021;10(3):2001256. doi:10.1002/adhm.202001256.
14. Zhan H, Ma F, Huang Y, Zhang J, Jiang X, Qian Y. Application of composite dissolving microneedles with high drug loading ratio for rapid local anesthesia. *Eur J Pharm Sci.* 2018;121:330-337.
15. Larrañeta E, Moore J, Vicente-Pérez EM, et al. A proposed model membrane and test method for microneedle insertion studies. *Int J Pharm.* 2014;472(1-2):65-73. doi:10.1016/j.ijpharm.2014.05.042.
16. Liu D, Yu B, Jiang G, Yu W, Zhang Y, Xu B. Fabrication of composite microneedles integrated with insulin-loaded CaCO<sub>3</sub> microparticles and PVP for transdermal delivery in diabetic rats. *Mater Sci Eng C.* 2018;90:180-188.
17. Yu W, Jiang G, Zhang Y, Liu D, Xu B, Zhou J. Polymer microneedles fabricated from alginate and hyaluronate for transdermal delivery of insulin. *Mater Sci Eng C.* 2017;80:187-196.
18. Raphael AP, Crichton ML, Falconer RJ, et al. Formulations for microprojection/microneedle vaccine delivery: Structure, strength and release profiles. *J Contr Release.* 2016;225:40-52.
19. Larrañeta E, Moore J, Vicente-Pérez EM, et al. A proposed model membrane and test method for microneedle insertion studies. *Int J Pharm.* 2014;472(1-2):65-73.
20. Aung NN, Ngawhirunpat T, Rojanarata T, Patrojanasophon P, Pamornpathomkul B, Opanasopit P. Fabrication, characterization and comparison of  $\alpha$ -arbutin loaded dissolving and hydrogel forming microneedles. *Int J Pharm.* 2020;586:119508.
21. Martanto W, Moore JS, Kashlan O, et al. Microinfusion using hollow microneedles. *Pharm Res (N Y).* 2006;23(1):104-113.
22. Li J, Zhou Y, Yang J, et al. Fabrication of gradient porous microneedle array by modified hot embossing for transdermal drug delivery. *Mater Sci Eng C.* 2019;96:576-582.
23. Donnelly RF, McCrudden MT, Zaid Alkilani A, et al. Hydrogel-forming microneedles prepared from "super swelling" polymers combined with lyophilised wafers for transdermal drug delivery. *PLoS One.* 2014;9(10):e111547.
24. Chaudhary B, Verma S. Preparation and evaluation of novel in situ gels containing acyclovir for the treatment of oral herpes simplex virus infections. *Sci World J.* 2014;2014:280928.
25. Ahmed A, Getti G, Boateng J. Ciprofloxacin-loaded calcium alginate wafers prepared by freeze-drying technique for potential healing of chronic diabetic foot ulcers. *Drug Deliv Translational Res.* 2018;8(6):1751-1768.
26. Khalid I, Ahmad M, Usman Minhas M, Barkat K, Sohail M. Cross-linked sodium alginate-g-poly (acrylic acid) structure: A potential hydrogel network for controlled delivery of loxoprofen sodium. *Adv Polym Technol.* 2018;37(4):985-995.
27. Vora LK, Vavia PR, Larrañeta E, Bell SE, Donnelly RF. Novel nanosuspension-based dissolving microneedle arrays for transdermal delivery of a hydrophobic drug. *J Interdiscipl Nanomed.* 2018;3(2):89-101.
28. Amodwala S, Kumar P, Thakkar HP. Statistically optimized fast dissolving microneedle transdermal patch of meloxicam: A patient friendly approach to manage arthritis. *Eur J Pharm Sci.* 2017;104:114-123.
29. Ronnander P, Simon L, Spilgies H, Koch A, Scherr S. Dissolving polyvinylpyrrolidone-based microneedle systems for in vitro delivery of sumatriptan succinate. *Eur J Pharmaceut Sci.* 2018;114:84-92.
30. González-Vázquez P, Larrañeta E, McCrudden MTC, et al. Transdermal delivery of gentamicin using dissolving microneedle arrays for potential treatment of neonatal sepsis. *J Contr Release.* 2017;265:30-40. doi:10.1016/j.jconrel.2017.07.032.
31. Shabbir M, Ali S, Farooq M, et al. Formulation factors affecting in vitro and ex vivo permeation of bisoprolol fumarate from a

- matrix transdermal patch. *Adv Polym Technol.* 2016;35(3): 237-247.
32. Donnelly RF, McCrudden MT, Zaid Alkilani A, et al. Hydrogel-forming microneedles prepared from “super swelling” polymers combined with lyophilised wafers for transdermal drug delivery. *PLoS One.* 2014;9(10):e111547. doi:10.1371/journal.pone.0111547.
  33. Shao C, Dowling TC, Haidar S, Yu L, Polli JE, Kane MA. Quantification of Acyclovir in human plasma by ultra-high-performance liquid chromatography - heated electrospray ionization - tandem mass spectrometry for bioequivalence evaluation. *J Anal Bioanal Tech.* 2012;03(139):1-6. doi:10.4172/2155-9872.1000139.
  34. Zhang Y, Huo M, Zhou J, Xie S. PKSolver: An add-in program for pharmacokinetic and pharmacodynamic data analysis in microsoft excel. *Comput Method Progr Biomed.* 2010;99(3): 306-314.
  35. Mistilis MJ, Bommarius AS, Prausnitz MR. Development of a thermostable microneedle patch for influenza vaccination. *J Pharmaceut Sci.* 2015;104(2):740-749.
  36. McAlister E, Kearney M-C, Martin EL, Donnelly RF. From the laboratory to the end-user: a primary packaging study for microneedle patches containing amoxicillin sodium. *Drug Deliv Transl Res.* 2021;11(5):2169-2185.
  37. Park J-H, Allen MG, Prausnitz MR. Polymer microneedles for controlled-release drug delivery. *Pharm Res.* 2006;23(5): 1008-1019.
  38. Lee JW, Park J-H, Prausnitz MR. Dissolving microneedles for transdermal drug delivery. *Biomaterials.* 2008;29(13):2113-2124.
  39. Aung NN, Ngawhirunpat T, Rojanarata T, Patrojanasophon P, Opanasopit P, Pamornpathomkul B. HPMC/PVP Dissolving microneedles: A promising delivery platform to promote trans-epidermal delivery of alpha-arbutin for skin lightening. *AAPS PharmSciTech.* 2020;21(1):25.
  40. Yu K, Yu X, Cao S, et al. Layered dissolving microneedles as a need-based delivery system to simultaneously alleviate skin and joint lesions in psoriatic arthritis. *Acta Pharm Sin B.* 2021;11(2): 505-519.
  41. McGrath MG, Vucen S, Vrdoljak A, et al. Production of dissolvable microneedles using an atomised spray process: Effect of microneedle composition on skin penetration. *Eur J Pharm Biopharm.* 2014;86(2):200-211.
  42. Tiron LG, Vlad M, Baltă Ș. Research on hydrophilic nature of polyvinylpyrrolidone on polysulfone membrane filtration. *IOP Conf Ser Mater Sci Eng.* 2018;374:012059. IOP Publishing.
  43. Ng KW, Lau WM. Skin deep: The basics of human skin structure and drug penetration. *Percutaneous Penetra Enhancers Chem Method Penetra Enhance.* 2015; 3-11. Springer.
  44. Stahl J, Wohlert M, Kietzmann M. Microneedle pretreatment enhances the percutaneous permeation of hydrophilic compounds with high melting points. *BMC Pharmacol Toxicol.* 2012;13(1):5.
  45. Foox M, Zilberman M. Drug delivery from gelatin-based systems. *Expet Opin Drug Deliv.* 2015;12(9):1547-1563.
  46. Casian T, Iurian S, Bogdan C, Rus L, Moldovan M, Tomuta I. QbD for pediatric oral lyophilisates development: Risk assessment followed by screening and optimization. *Drug Develop Indust Pharm.* 2017;43(12):1932-1944.
  47. Tang XC, Nail SL, Pikal MJ. Freeze-drying process design by manometric temperature measurement: design of a smart freeze-dryer. *Pharm Res.* 2005;22(4):685-700.
  48. Pawar HV, Boateng JS, Ayensu I, Tetteh J. Multifunctional medicated lyophilised wafer dressing for effective chronic wound healing. *J Pharmaceut Sci.* 2014;103(6):1720-1733.
  49. Malik NS, Ahmad M, Minhas MU. Cross-linked  $\beta$ -cyclodextrin and carboxymethyl cellulose hydrogels for controlled drug delivery of acyclovir. *PLoS One.* 2017;12(2):e0172727.
  50. da Almeida PF, da Silva Lannes SC, Calarge FA, da Brito Farias TM, Santana JCC. FTIR characterization of gelatin from chicken feet. *J Chemis Chem Eng.* 2012;6(11):1029.
  51. Rajbanshi K, Bajracharya R, Shrestha A, Thapa P. Dissolution enhancement of aceclofenac tablet by solid dispersion technique. *Int J Pharma Sci Res.* 2014;5(4):127-139.
  52. Jayaramudu T, Varaprasad K, Pyarasani RD, et al. Hydroxypropyl methylcellulose-copper nanoparticle and its nanocomposite hydrogel films for antibacterial application. *Carbohydr Polym.* 2021;254:117302.
  53. Karavas E, Georgarakis E, Bikiaris D. Adjusting drug release by using miscible polymer blends as effective drug carries. *J Ther Analysis Calorim.* 2006;84(1):125-133.
  54. McPhillips H, Craig DQM, Royall PG, Hill VL. Characterisation of the glass transition of HPMC using modulated temperature differential scanning calorimetry. *Int J Pharm.* 1999; 180(1):83-90.
  55. Abdelrazek E, Ragab H, Abdelaziz M. Physical characterization of poly (vinyl pyrrolidone) and gelatin blend films doped with magnesium chloride. *Plastic Polymer Technol.* 2013;2(1):1-8.
  56. Mohamed HB, El-Shanawany SM, Hamad MA, Elsabahy M. Niosomes: A strategy toward prevention of clinically significant drug incompatibilities. *Sci Rep.* 2017;7(1):6340-6414.
  57. Ghorani B, Emadzadeh B, Rezaeinia H, Russell SJ. Improvements in gelatin cold water solubility after electrospinning and associated physicochemical, functional and rheological properties. *Food Hydrocolloids.* 2020;104:105740.
  58. Nguyen T-H, Lee B-T. Fabrication and characterization of cross-linked gelatin electro-spun nano-fibers. *J Biomed Sci Eng.* 2010; 03(12):1117-1124.
  59. Jaipal A, Pandey M, Charde S, Raut P, Prasanth K, Prasad R. Effect of HPMC and mannitol on drug release and bioadhesion behavior of buccal discs of buspirone hydrochloride: In-vitro and in-vivo pharmacokinetic studies. *Saudi Pharmaceut J.* 2015;23(3):315-326.
  60. Yalçın Ş, Mutlu I. Structural characterization of some table salt samples by XRD, ICP, FTIR and XRF techniques. *Acta Physica Polonica-Series A General Phy.* 2012;121(1):50.
  61. Avachat AM, Takudage PJ. Design and characterization of multifaceted lyophilized liposomal wafers with promising wound healing potential. *J Liposome Res.* 2018;28(3):193-208.

62. Mruthyunjaya Swamy TM, Ramaraj B, Hatna S. Thermal and morphological properties of SA/HPMC blends. *J Appl Polym Sci.* 2009;112(4):2235-2240.
63. Betti NA. Thermogravimetric analysis on PVA/PVP blend under air atmosphere. *Eng Technol J.* 2016;34(13):2433-2441.
64. Gasaymeh SS, Radiman S, Heng LY, Saion E, Saeed GM. Synthesis and characterization of silver/polyvinylpyrrolidone (Ag/PVP) nanoparticles using gamma irradiation techniques. *Af Rev of Phy.* 2010;4:0006.
65. Derya Ü. Pervaporative desalination of water using hydroxypropyl methylcellulose/polyvinylpyrrolidone blend membranes. *J Innovative Sci Eng.* 2020;4(1):35-43.
66. Shamsipur M, Pourmortazavi SM, Beigi AAM, Heydari R, Khatibi M. Thermal stability and decomposition kinetic studies of acyclovir and zidovudine drug compounds. *AAPS PharmSciTech.* 2013;14(1):287-293.
67. Kumaresan G, Velraj R, Iniyar S. Thermal analysis of D-mannitol for use as phase change material for latent heat storage. *J Appl Sci.* 2011;11(16):3044-3048.
68. Yang X, Lu J, Wang X-J, Ching C-B. Effect of sodium chloride on the nucleation and polymorphic transformation of glycine. *J Cryst Growth.* 2008;310(3):604-611.
69. Matthews KH, Stevens HN, Auffret AD, Humphrey MJ, Eccleston GM. Formulation, stability and thermal analysis of lyophilised wound healing wafers containing an insoluble MMP-3 inhibitor and a non-ionic surfactant. *Int J Pharm.* 2008;356(1-2):110-120.
70. Kim SE, Heo DN, Lee JB, et al. Electrospun gelatin/polyurethane blended nanofibers for wound healing. *Biomed Mater.* 2009;4(4):044106.
71. Kianfar F, Ayensu I, Boateng JS. Development and physico-mechanical characterization of carrageenan and poloxamer-based lyophilized matrix as a potential buccal drug delivery system. *Drug Develop Indust Pharm.* 2014;40(3):361-369.
72. Farias S, Boateng JS. Development and functional characterization of composite freeze dried wafers for potential delivery of low dose aspirin for elderly people with dysphagia. *Int J Pharm.* 2018;553(1-2):65-83.
73. Ruela ALM, Perissinato AG, Lino MEdS, Mudrik PS, Pereira GR. Evaluation of skin absorption of drugs from topical and transdermal formulations. *Braz J Pharm Sci.* 2016;52(3):527-544.
74. Chu KR, Lee E, Jeong SH, Park E-S. Effect of particle size on the dissolution behaviors of poorly water-soluble drugs. *Arch Pharm Res (Seoul).* 2012;35(7):1187-1195.
75. El-Massik M, Darwish I, Hassan E, El-Khordagui L. Development of a dissolution medium for glibenclamide. *Int J Pharm.* 1996;140(1):69-76.
76. Taupitz T, Klein S. Can biorelevant media be simplified by using SLS and Tween 80 to replace bile compounds? *Open Drug Deliv J.* 2010;4(1):30-37.
77. Soni T, Nagda C, Gandhi T, Chotai N. Development of discriminating method for dissolution of aceclofenac marketed formulations. *Dissolution Technol.* 2008;15(2):31-35.
78. Nair AB. Quantification of uptake and clearance of acyclovir in skin layers. *Antivir Ther.* 2015;21(1):17-25.
79. Alshehri S, Hussain A, Altamimi MA, Ramzan M. In vitro, ex vivo, and in vivo studies of binary ethosomes for transdermal delivery of acyclovir: A comparative assessment. *J Drug Deliv Sci Technol.* 2021;62:102390.
80. Liu H, Qiu K, He Q, Lei Q, Lu W. Mechanisms of blood-brain barrier disruption in herpes simplex encephalitis. *J Neuroimmune Pharmacol.* 2019;14(2):157-172.
81. Kondel R, Shafiq N, Kaur IP, et al. Effect of acyclovir solid lipid nanoparticles for the treatment of herpes simplex virus (HSV) infection in an animal model of HSV-1 infection. *Pharm Nanotechnol.* 2019;7(5):389-403.
82. Smith R, Morroni J, Wilcox C. Lack of effect of treatment with penciclovir or acyclovir on the establishment of latent HSV-1 in primary sensory neurons in culture. *Antivir Res.* 2001;52(1):19-24.
83. Deshmukh K, Ahamed MB, Deshmukh R, Khadheer Pasha SK, Bhagat PR, Chidambaram K. Biopolymer composites with high dielectric performance: interface engineering. *Biopolymer Compos Electr.* 2017; 27-128. Elsevier.